Article:
Dai, X, Song, H, Wignall, PB et al. (2018) Rapid biotic rebound during the late Griesbachian indicates heterogeneous recovery patterns after the Permian-Triassic mass extinction. GSA Bulletin, 130 (11-12). pp. 2015-2030. ISSN: 0016-7606

https://doi.org/10.1130/B31969.1

Rapid biotic rebound during the late Griesbachian indicates heterogeneous recovery patterns after the Permian-Triassic mass extinction

Xu Dai[1], Haijun Song[1*], Paul B. Wignall[2], Enhao Jia[1], Ruoyu Bai[1], Fengyu Wang[1], Jing Chen[3], Li Tian[1]

[1]*State Key Laboratory of Biogeology and Environmental Geology, School of Earth Sciences, China University of Geosciences, Wuhan 430074, China*

[2]*School of Earth and Environment, University of Leeds, Leeds LS2 9JT, UK*

[3]*Yifu Museum of China University of Geosciences, Wuhan 430074, China*

*Corresponding author. Email: haijun.song@aliyun.com

ABSTRACT

New fossil data of two Early Triassic (Griesbachian to Dienerian) sections from South China show unusually high levels of both benthic and nektonic taxonomic richness, occurring in the late Griesbachian. A total of 68 species (including 26 species of Triassic-type species) representing mollusks, brachiopods, foraminifers, conodonts, ostracods, and echinoderms occur in the late Griesbachian, indicating well-established and relatively complex marine communities. Furthermore, the nekton shows higher origination rates than the benthos. Analyses of sedimentary facies and size distribution of pyrite framboids show that this high-diversity interval is associated with well-oxygenated environments. In contrast to the previously suggested scenario that persistently harsh environmental conditions impeded the biotic recovery during the

Early Triassic, our new findings, combined with recent works, indicate a fitful regional recovery pattern after the Permian-Triassic crisis resulting in three main diversity highs: late Griesbachian-early Dienerian, early-middle Smithian and Spathian. The transient rebound episodes are therefore influenced by both extrinsic local (e.g. redox condition, temperature) and intrinsic (e.g. biological tolerances, origination rate) parameters.

INTRODUCTION

The Permian-Triassic mass extinction (PTME) was the largest biotic catastrophe of the Phanerozoic, which eliminated around 80% to 90% of marine species (Raup, 1979; Song et al., 2013; Stanley, 2016) and heralded the development of modern ecosystems (Sepkoski, 1981; Brayard et al., 2017). After this mass extinction, depauperate faunas were prevailed throughout the Early Triassic, and not until the Middle Triassic did diversity rebound (Erwin and Pan, 1996; Nützel, 2005; Payne et al., 2006; Tong et al., 2007). The delay has been attributed to the magnitude of the PTME and the evolution to replace the losses (e.g. Erwin, 2001). Alternatively, persistent environmental disturbances in the Early Triassic have been held responsible such as marine anoxia (Algeo et al., 2007, 2008; Bond and Wignall, 2010; Song et al., 2012; Tian et al., 2014; Clarkson et al., 2016; Lau et al., 2016; Wignall et al., 2016), high temperatures (Sun et al., 2012; Romano et al., 2013), elevated atmospheric CO_2 (Fraiser and Bottjer, 2007), and abnormal productivity (Algeo et al., 2011; Meyer et al., 2011; Grasby et al., 2016). Additionally, the 'Lilliput effect' (dwarfism of surviving organisms) was also pervasive among many clades during the Early Triassic, e.g. foraminifers (Payne et al., 2011; Song et al., 2011), ostracods (Chu et al., 2015), bivalves (Twitchett,

45 2007), gastropods (Payne, 2005), and brachiopods (He et al., 2015). However, the
46 spatiotemporal extent and significance of this phenomenon are debated (see e.g.,
47 Brayard et al., 2010, 2015; Forel and Crasquin, 2015).

48 Contrary to the prolonged recovery scenario, recent studies on conodonts,
49 ammonoids and foraminifers reveal a fitful recovery pattern that shows diversification
50 was not underway until the Smithian (Orchard, 2007; Brayard et al., 2009; Song et al.,
51 2011), less than ~1.5 million years after the PTME. Recovery was then setback by a
52 severe crisis in the late Smithian (Brayard et al., 2006; Stanley, 2009). Data from Oman
53 (Krystyn et al., 2003; Twitchett et al., 2004), Italy (Hofmann et al., 2011, 2015; Foster
54 et al., 2017), the Northern Indian Margin (Brühwiler et al., 2010; Wasmer et al., 2012;
55 Kaim et al., 2013; Ware et al., 2015;), South Primorye (Shigeta et al., 2009), western
56 USA (Brayard et al., 2013, 2015, 2017; Hautmann et al., 2013; Hofmann et al., 2013,
57 2014), South China (Chen et al., 2007; Brayard and Bucher, 2008; Kaim et al., 2010;
58 Hautmann et al., 2011; 2015; Wang et al., 2017), and Svalbard (Foster et al., 2016) also
59 documented spatiotemporally variable diversification and occurrences of rather
60 complex communities. However, few of these works provide exhaustive correlation
61 between paleontological and environmental data to decipher the recovery course and
62 its controlling factors. In many regions, marine environments were apparently
63 depauperate during the Griesbachian-Dienerian with local exceptions (e.g. Twitchett et
64 al., 2004). Such occurrences are considered to have become more common in the
65 Spathian (Pietsch and Bottjer, 2014). Thus, the overall spatiotemporal pattern and the
66 clade variability of the biotic recovery following the PTME are still unclear and

67 therefore controversial, as well its environmental drivers.

68 Sampling efforts and preservation biases influence our knowledge of the biotic
69 recovery. For instance, Early Triassic silicified fossil assemblages are quite rare, but
70 show relatively high diversity when present (Foster et al., 2016). Extensive sampling
71 efforts and new findings might change our understanding of biotic recovery model (e.g.
72 Brayard et al., 2015, 2017). So far, no hypothesis has addressed the question of why the
73 re-diversification of a few clades (e.g. ammonoids and conodonts) were more rapid,
74 while others were rather slow (e.g. brachiopods). Recent studies showed that
75 environmental conditions (e.g. temperature, oxygen concentration) strongly fluctuated
76 in the Early Triassic (Algeo et al., 2011; Song et al, 2012; Sun et al, 2012; Grasby et al.,
77 2013; Tian et al., 2014), but only rarely have studies tried to link such environmental
78 fluctuations to observed recovery patterns amongst clades (e.g. Pietsch et al. 2014).
79 South China provides one of the best marine fossil records of the Permian-Triassic
80 transition, and often serves as an example of the prolonged recovery scenario (e.g.,
81 Payne et al., 2006; Tong et al., 2007). However, recent reports of unusually diverse
82 earliest Triassic faunas from Guangxi (Kaim et al. 2010; Hautmann et al. 2011) question
83 this model. Here we provide new paleontological and paleoenvironmental data from
84 two Griesbachian-Dienerian sections in Guizhou and Hubei provinces, South China,
85 that record relatively high diversity levels among several groups and their associated
86 paleoenvironmental indicators as potential biotic change drivers.

87 **GEOLOGICAL SETTING**

88 During the Early Triassic, the South China Block was located in equatorial

89 latitudes, at the interface between Panthalassa and Tethys (Fig. 1A). Marine Lower
90 Triassic sediments are widespread especially the carbonates of the Yangtze Platform.
91 This platform was located centrally in the South China Block, and adjacent to the
92 Nanpanjiang Basin (Fig. 1B). The platform successions are divided into the Daye
93 Formation, dominated by limestones, and the overlying Jialingjiang Formation,
94 composed of dolomites (Feng et al., 1997). Lower Triassic strata of the Nanpanjiang
95 Basin consists of basinal clastic and carbonate rocks plus shallower carbonates of
96 limited area which formed on isolated platforms (Feng et al., 1997; Bagherpour et al.,
97 2017). The two studied sections (Gujiao and Jianzishan) were located at the southern
98 and northern sides of the Yangtze Platform margin, respectively (Fig. 1B).

99 **Gujiao section**

100 The Gujiao section (26º30′49.22″N, 106º52′15.17″E) is located ~20 km east from
101 Guiyang and was situated in the transitional zone between the Nanpanjiang Basin and
102 the Yangtze Platform during the Early Triassic (Fig. 1B). A new and well-exposed
103 outcrop was found in 2015 along a newly-built road, close to the Gujiao County,
104 showing a continuous Permian-Triassic succession (Fig. 2A). The Upper Permian
105 Changxing Formation is dominated by light gray, bioclastic limestones, and yields
106 abundant and diverse Permian organisms including brachiopods, gastropods, corals,
107 dasycladacean algae, and foraminifers. The overlying Dalong Formation consists of
108 cherty mudstones and black shales, with occasionally volcanic ash beds, representing a
109 deeper basinal environment. The Dalong Formation contains abundant radiolarian
110 (Feng and Algeo, 2014; Xiao et al., 2017) and ammonoid (Zheng, 1981) faunas that

111 indicate a late Changhsingian age. The Lower Triassic Daye Formation conformably
112 overlies the Dalong Formation, and is dominated by marlstones alternating with shales
113 (Fig. 2B, C). The Permian-Triassic boundary is roughly correlated with the boundary
114 between the Dalong and Daye formations. Ammonoids are very abundant in the lower
115 part of Daye Formation. Dai et al. (submitted) identified three ammonoid beds in this
116 interval, the late Griesbachian *Ophiceras medium* and *Jieshaniceras guizhouense* beds,
117 and the middle Dienerian *Ambites radiatus* bed. The exact position of the
118 Griesbachian/Dienerian boundary is not well defined at Gujiao, but is likely just above
119 the *Jieshaniceras guizhouense* beds.

120 **Jianzishan section**

121 The Jianzishan (30º9′58.08″N, 109º0′27.5″E) section found ~20 km south of
122 Lichuan in Hubei Province, was located on the north margin of the Yangtze Platform
123 (Fig. 1B). The Late Permian and Early Triassic are represented by the Changxing and
124 Daye formations respectively. The former consists of thick-bedded bioclastic
125 limestones and calcareous sponge reefs with associated shallow-marine fossils (e.g.
126 corals, calcareous algae and fusulinids). The diverse fauna includes nautiloids,
127 foraminifers, dasycladacean algae, sponges, corals, and brachiopods (Liu et al., 2017).
128 The lowermost part of the Daye Formation is a 2.4 m thick microbialite (Fig. 2D), a
129 typical representative of the extensive microbial deposits found in the lowermost
130 Triassic strata of South China (e.g. Lehrman, 1999; Yang et al., 2011; Bagherpour et al.,
131 2017). The overlying strata are dominated by alternations of thin-bedded marlstones
132 and shales (Fig. 2E) that yield abundant bivalves, brachiopods (Wang et al., 2017) and

ammonoids, suggestive of an outer platform facies. Two ammonoid beds, the late Griesbachian *Ophiceras* sp. indet. and *Jieshaniceras guizhouense* beds are known (Bai et al., 2017). Four conodont zones, the late Changhsingian *Clarkina changxingensis* Zone and *Clarkina yini* Zone, the Griesbachian *Hindeodus parvus* Zone and the *Hindeodus postparvus* Zone, were found in the Jianzishan section (Bai et al., 2017). Strata between the *H. parvus* and the *H. postparvus* zones are not well dated by conodonts or ammonoids. Consequently, we here use the presence of abundant *Sinolingularia* to denote the assemblage at this level.

MATERIAL AND METHODS

Macrofossils (e.g., ammonoids and bivalves) were collected by mechanically breaking up decimeter-sized blocks. Mechanical techniques, including air and electrical scribes, were later performed in the laboratory to excavate morphologic details and thereby facilitate species-level identification. Specimens were photographed using a Canon 70D camera with a Micro lens EF 100mm f/2.8.

A total of 39 and 38 thin sections have been made to study microfossils from the Gujiao and Jianzishan sections, respectively. In addition, 16 and 18 samples were respectively collected from the Gujiao and Jianzishan sections for analyses of the size distribution of pyrite framboids. A polished slab (~1 × 1 cm) of each sample was examined for size measurements of pyrite framboids using a Scanning Electronic Microscope (SEM; Hitachi SU8000) at the State Key Laboratory of Biogeology and Environmental Geology in Wuhan, China. Paleoenvironmental factors have been investigated including local redox conditions determined using pyrite framboid size

155 analysis, following the approach of Bond and Wignall (2010). A minimum of 100 pyrite
156 framboids were measured when possible, according to the procedure of Huang et al.,
157 (2017).

158 **PALEONTOLOGICAL RESULTS**

159 Over 3500 specimens were collected from the Gujiao and Jianzishan sections (Figs
160 3, 4, Tables 1, 2), including ammonoids, nautiloids, bivalves, gastropods, brachiopods,
161 ostracods, echinoids, foraminifers, and conodonts. Paleozoic holdover and new
162 originated genus and species (species that belongs to new originated genus) are used
163 to qualitatively assess the composition of the biotas.

164 **Ammonoids**

165 Thirteen ammonoid species occur in the lower Daye Formation at the Gujiao
166 section, and seven ammonoid species occur in the lower Daye Formation from the
167 Jianzishan section (Bai et al., 2017). All ammonoid taxa from the two sections are new
168 originated. At Gujiao, five species (*Ophiceras medium*, Ophiceratidae gen. indet.,
169 Gyronitidae gen. indet., *Vishnuites pralambha* and ?Mullericeratidae gen. indet.) were
170 found in the *Ophiceras medium* beds. Five species (*Vishnuites pralambha*, *Ophiceras*
171 sp. indet., *Mullericeras* sp. nov., *Jieshaniceras guizhouense* and *Proptychites* sp. indet.)
172 were identified in the *Jieshaniceras guizhouense* beds. Four species (*Ambites radiatus*,
173 *Pseudoproptychites* cf. *hiemalis*, ?Gyronitidae gen et sp. nov and ?*Ussuridiscus* cf.
174 *varaha*) occur in the *Ambites radiatus* bed. At Jianzishan, only one taxon was found in
175 the *Ophiceras* sp. indet. beds. Six species (*Vishnuites pralambha*, *Ussuridiscus varaha*,
176 *Jieshaniceras guizhouense*, ?Gyronitidae gen. et sp. nov, *Hubeitoceras yanjiaensis* and

177 *Shangganites* sp. indet.) occur in the *Jieshaniceras guizhouense* beds.

178 Two successive ammonoid diversity levels are thus obvious: 1) a relatively high
179 species richness during the late Griesbachian, and 2) a relatively low species richness
180 level in the middle Dienerian, with a minimum richness above that. At Jianzishan, no
181 ammonoids were found in strata overlying the *Jieshaniceras guizhouense* beds.

182 **Nautiloids**

183 Nautiloids show a weak diversity level during the late Griesbachian (Fig. 5). Two
184 new originated nautiloids (*Xiaohenautilus huananensis* and *X. sinensis*) were identified
185 in the *Ophiceras medium* and *Jieshaniceras guizhouense* beds at the Jianzishan section.
186 Except for these two species, an unidentified nautiloid was also found in the
187 *Jieshaniceras guizhouense* beds at the Gujiao section. It mainly differs from
188 *Xiaohenautilus* by marked ribs on its flanks (Fig. 5). *X. huananensis* and *X. sinensis*
189 also occur in the *Jieshaniceras guizhouense* beds at Jianzishan.

190 **Bivalves**

191 At Gujiao, only three beds yield well preserved bivalves. A bed ~ 20 cm below the
192 middle Dienerian *Ambites radiatus* bed shows abundant bivalves identified as *Claraia*
193 *stachei*. The *Ambites radiatus* bed contains moderately abundant *Claraia radialis*, and
194 the overlying beds have abundant *Claraia aurita* (Fig. 6). These three *Claraia* species
195 belong to Paleozoic holdovers.

196 Seven bivalve species were found at Jianzishan (Figs. 6, 7): three species (*Claraia*
197 sp. indet., *Claraia wangi* and *Eumorphotis venetiana*) in the *Sinolingularia* beds, six
198 species (*C. wangi*, *C. zhenanica, E. venetiana*, *Eumorphotis* sp. indet., *Pteria ussurica*

199 *variabilis*, and *Scythentolium scutigerulus*) in the *Ophiceras* sp. indet. beds and two
200 species (*C.* sp. indet. and *C. zhenanica*) in the *Jieshaniceras guizhouense* beds. Three
201 of the species are new originated: *Eumorphotis venetiana*, *Eumorphotis* sp. indet. and
202 *Scythentolium scutigerulus*. The *Ophiceras* sp. indet. beds contain the most diverse and
203 abundant bivalves.

204 **Gastropods**

205 Gastropods specimens are poorly preserved at both sections (Fig. 8). Thus, their
206 taxonomic assignment is often tentative. Identifications were mainly based on their
207 shell height and width, and number of whorls. We also categorized studied specimens
208 under the following designation 'unidentified gastropod A, B, C, etc'. to distinguish
209 them when necessary.

210 At least seven species are present at Jianzishan, two (Bellerophontidae gen. indet.
211 and unidentified gastropod A) in the *Hindeodus parvus* Zone, one (Bellerophontidae
212 gen. indet.) in the *Sinolingularia* beds, two (Bellerophontidae gen. indet.
213 and ?*Pseudomurchisonia* sp. indet) in the *Ophiceras* sp. indet. beds and three
214 (unidentified gastropods A, B and C) in the *Jieshaniceras guizhouense* beds.

215 At Gujiao, four gastropods species were found, three (?*Naticopsis* sp. indet.,
216 unidentified gastropods D, E) in the *Ophiceras medium* beds, four (?*Naticopsis* sp.
217 indet., Bellerophontidae gen. indet. and unidentified gastropods D, E) in the
218 *Jieshaniceras guizhouense* beds, and one (unidentified gastropod E) in the *Ambites*
219 *radiatus* bed. Gastropods are absent in the overlying beds. In summary, gastropods are
220 abundant in the late Griesbachian *Ophiceras medium* and *Jieshaniceras guizhouense*

beds, but seemingly displaya low diversity.

Brachiopods

Only one brachiopod species (*Lichuanorelloide lichuanensis*) was excavated from the *Jieshaniceras guizhouense* beds at Gujiao, whilst five brachiopods species (including three articulated brachiopods) were recognized at Jianzishan. *Sinolingularia* sp. indet. is very abundant in the *Sinolingularia* beds (Fig. 7). The *Ophiceras* sp. indet. beds contain two brachiopods species (*Crurithyris* sp. indet. and *Lingularia* sp. indet., Fig. 7) and the *Jieshaniceras guizhouense* beds have a relatively diverse brachiopod fauna with five identified species (*Sinolingularia* sp. indet., *Lingularia* sp. indet., *Crurithyris* sp. indet., *Lichuanorelloide lichuanensis* and *Lissorhynchia* sp. indet.). Among these five species, three (*Sinolingularia* sp. indet., *Lichuanorelloide lichuanensis* and *Lissorhynchia* sp. indet.) are new originated, and suggest a notable brachiopod diversification after the PTME (Wang et al., 2017).

Foraminifers

A total of 20 species were identified in the Gujiao and Jianzishan sections (Fig. 9). At Gujiao, seven species (*Nodosinelloides* sp. indet., *Gaudryina* sp. indet., *Dentalina* sp. indet., *Tolypammina* sp. indet., *Glomospira* sp. indet., *Duotaxis* sp. indet. and ?*Dagmarita* sp. indet.) occur in the *Ophiceras medium* beds, and ten (*Nodosinelloides* sp. indet., *Gaudryina* sp. indet., *Dentalina* sp. indet., *Tolypammina* sp. indet., *Glomospira* sp. indet., *Duotaxis* sp. indet., ?*Dagmarita* sp. indet., *Geinitzina* sp. indet., ?*Vervilleina* sp. indet. and *Nodosaria* sp. indet.) in the *Jieshaniceras guizhouense* beds. Two species are new originated, *Gaudryina* sp. indet. and *Duotaxis* sp. indet.

Overall, foraminiferal species richness was relatively high during the late Griesbachian, whereas no foraminifer specimens were retrieved from the overlying Dienerian strata.

At Jianzishan, 12 species (*Earlandia* sp. indet., *Postcladella kalhori*, *Ammodiscus* sp. indet., *Dentalina* sp. indet., "*Nodosaria*" sp. indet., *Tezaquina* sp. indet., *Heimigordius* sp. indet., *Nodosinelloides* sp. indet., ?*Duotaxis* sp. indet., *Geinitzina* sp. indet., "*Nodosaria*" *elabugae* and "*Nodosaria*" *skyphica*) were found in the *Hindeodus parvus* Zone, but no foraminifer specimens were found in the *Sinolingularia* beds and *Ophiceras* sp. indet. beds. Eight species (*Postcladella kalhori*, *Nodosinelloides* sp. indet., *Geinitzina* sp. indet., *Glomospira* sp. indet., *Tolypammina* sp. indet., *Frondina* sp. indet., *Vervilleina* sp. indet. and *Nodosinelloides sagitta*) occur in the *Jieshaniceras guizhouense* beds. All these species belong to Paleozoic holdovers.

PYRITE FRAMBOID RESULT AND PALEOREDOX INTERPRETATION.

Gujiao section

At Gujiao, five of the 16 samples exhibit abundant framboids, whereas the rest contained few or no pyrite framboids (Fig. 10). Framboids in samples GJ-f and GJ-11 display a small mean diameter (3.15 μm and 4.76 μm respectively), as well as small standard deviations (1.14 and 2.66 respectively; Fig. 11). These measurements suggest euxinic-anoxic conditions for these beds (Fig. 12), based on the approach of Bond and Wignall (2010) and Tian et al. (2014). Nine samples from the *Ophiceras medium* and *Jieshaniceras guizhouense* beds yield few or no framboids. Three of the remaining six samples from the overlying Dienerian strata show occurrences of framboids (Fig. 10). Only one sample, (GJ-40) from the *Ambites radiatus* bed, is dominated by small

framboids, with a small mean diameter and standard deviation (MD = 4.76 μm, SD = 1.98; Fig. 11), indicating euxinic-anoxic condition (Fig. 12). Above this bed, two samples (GJ-III-5+0.2 and GJ-III-5+0.9) yield abundant framboids, with a larger mean diameter, about 5.8 μm (Fig. 11). These plot in the weakly dysoxic (GJ-III-5+0.2) and anoxic fields (GJ-III-5+0.9) in figure 12 which is calibrated from studies of modern environments that record a range of redox-related regimes (Bond and Wignall, 2010).

The paleoredox trends derived from pyrite framboid size distributions are congruent with occurrences of trace fossils and the observed succession of facies (Figs 2, 13). Anoxic and dysoxic intervals, inferred from framboid data, coincide with an absence of bioturbation and correspond to dark, thin-bedded, finely laminated marlstones interbedded with black shales (Fig. 2B). The beds with rare or no pyrite framboids are dominated by light-gray, thin bedded marlstones (Fig. 2C) with abundant vertical tracers *Arenicolites* (Fig. 13A).

Jianzishan section

At Jianzishan, only two samples (JZS-2+1.1 and JZS-2+2.1) from the basal Triassic microbialites yield moderately abundant, large pyrite framboids, whereas framboids were rare or absent in other samples (Fig. 10). Both framboid populations exhibit diameters and standard deviations that plot in dysoxic fields (Fig. 12). Other samples lack pyrite framboids and likely indicate oxic conditions during deposition of the *Sinolingularia*, *Ophiceras* sp. indet. and *Jieshaniceras guizhouense* beds. Moderately abundant vertical ichnofossils (e.g. *Skolithos*) occur in the *Jieshaniceras guizhouense* beds (Fig. 13B), also suggesting well-oxygenated conditions.

DISCUSSION

Late Griesbachian rapid recovery

Previous works in South China support the claims of a delayed recovery in China caused by persisting environmental stresses up until at least the Spathian (e.g. Payne et al., 2006; Tong et al., 2007; Sun et al., 2012; Song et al., 2012). Chen et al. (2007) documented a rapid onset of recovery at Meishan section, however, only nine species of macrofossils were found during late Griesbachian. Our data show that moderately diverse marine communities flourished soon after the PTME, during the late Griesbachian, at least in well-oxygenated environments. Rarefaction analyses indicate that the highest diversity is in the *Jieshaniceras guizhouense* beds both at Gujiao and Jianzishan (Fig. 14). Furthermore, the microbialite community (early Griesbachian) is rather diverse at Jianzishan that likely results from the non-lethal oxygen poor conditions and supports the microbialites refuge model (Forel et al., 2013). At Gujiao, the early Griesbachian witnessed depressed marine community under anoxic-euxinic conditions in the aftermath of PTME. The diversity in the *Jieshaniceras guizhouense* beds at Gujiao is lower than that at Jianzishan, 26 and 37 species at Gujiao and Jianzishan respectively, supporting that redox condition plays a significant role in diversity rebound. There is no marked shift in facies observed near the Griesbachian/Dienerian boundary at the both sections indicating that the dramatic diversity reduction after the late Griesbachian is not a bias resulting from major facies change. However, the causation of this small crisis still needs more work to decipher.

At Jianzishan, a marked Paleozoic holdovers diversity drop is observed between

309 the *Hindeodus parvus* Zone and *Sinolingularia* beds (Figs 4, 15), possibly reflecting
310 the second pulse of the PTME in the earliest Triassic mass extinction (Song et al., 2013).
311 Alternatively (or additionally), this diversity loss might be related to the facies shift
312 between the microbialites and mudstones (Fig. 4). High diversity levels of Paleozoic
313 holdovers and new originated taxa occurred during the late Griesbachian in both
314 sections. Additionally, during the late Griesbachian, nektonic taxa show a more marked
315 rebound than benthic organisms, e.g. ammonoid (proptychitids). This difference
316 between nektonic and benthic taxa may result from the relatively stronger mobility of
317 nektonic organisms such as cephalopods, which makes them better able to avoid
318 spatially variable hostile environments (Bambach et al., 2002). However, it could also
319 reflect the intrinsically evolutionary rate of ammonoids that tends to be high, compared
320 to other mollusk groups, at all times during the clades' history (Stanley, 2009).
321 Well-oxygenated conditions during the late Griesbachian have rarely been
322 documented in South China, and the interval is widely reported to be poorly ventilated
323 in marine settings (Song et al., 2012; Tian et al., 2014; Huang et al., 2017; Li et al.,
324 2016). Our data reveal that there were heterogeneous redox conditions at this time.
325 Gujiao and Jianzishan sections were located on the platform margin, a predicted
326 "Refuge Zone" sandwiched beneath the potentially warm surface waters and anoxic
327 deeper waters (Song et al. 2014; Godbold et al., 2017). Our results suggest that diversity
328 patterns in the Early Triassic were strongly controlled by the presence of anoxia, with
329 recovery best seen in the limited areas of more ventilated conditions (Fig. 15).
330 Similar high diversity levels rapidly after the PTME are also known from a limited

number of other locations. For example, a late Griesbachian fauna with ammonoids, bivalves and gastropods in oxic strata is seen in Oman (Krystyn et al., 2003; Twitchett et al., 2004). The overall diversity during Griesbachian and Dienerian at Meishan section is relative high, probably owing to its overmuch studies, especially near the Permian-Triassic boundary. In addition, the diverse conodont fauna contributes the most of overall diversity (Zhang et al., 2007). However, the low diversity of mollusk taxa and oxygen poor conditions during the late Griesbachian at Meishan also support that redox condition is a key factor in controlling biotic recovery (Chen et al., 2007, 2014; Li et al., 2016). The Siusi Member (late Griesbachian-Dienerian) of the Werfen Formation (Dolomites, Italy) also yields relatively diverse mollusk communities in well oxygenated environment (Wignall and Twitchett, 1996; Hofmann et al., 2015; Foster et al., 2017). A marked ammonoid diversity richness has been documented in the Northern Indian Margin (Salt Range and Spiti) during the early Dienerian (Ware et al., 2015), and this interval was proved to be well oxygenated (Hermann et al., 2011). Combination of the works above and present work support the heterogeneous recovery pattern and rapid diversification only present under oxic conditions.

Several studies described diverse mollusk faunas from the earliest Triassic microbialites of South China (Kaim et al., 2010; Hautmann et al., 2011, 2015). The microbialites may have serve as a refuge for benthic organisms (e.g., Forel et al., 2013), but reconstructions of paleoredox conditions within these deposits suggests variety of redox conditions (e.g. Forel et al., 2009, 2013; Liao et al., 2017). However, these microbialites occur between the two phases of the PTME (Jiang et al., 2014; Brosse et

al., 2015) that straddle the Permian-Triassic boundary (Song et al., 2013), and thus record intra-extinction conditions not those during the recovery. It is noteworthy that the most microbialite taxa are Paleozoic holdovers (Hautmann et al., 2015), and so just record assemblages that survived the first (but not the second) stage of the PTME.

In South China, biotic recovery was impeded by anoxic events later in the Dienerian (Figs. 10, 15), as also seen in other basins, e.g. Pakistan (Hermann et al., 2011) and northern Italy (Foster et al., 2017). Overall, previous works and our results suggest that recovery after the PTME was spatiotemporally heterogeneous and highly dependent on local environmental conditions as seen during the late Griesbachian in our two studied sections with same sample effort and similar preservation conditions in South China. The most abundant and diversified Griesbachian communities were to be in shallower (but not the shallowest) and more oxic settings.

Fitful recovery pattern

Based on our new data and previous studies, a fitful recovery pattern from the PTME can be simplified into three distinct phases of relatively high diversity that vary in time and space according to regional and local environmental conditions: I. late Griesbachian-early Dienerian; II. early-middle Smithian and III. Spathian. During phase I, new originated genus became the dominant group in South China, especially amongst the ammonoid-dominated nektonic communities. This recovery phase was short-lived and probably curtailed by the return of anoxic conditions during the Dienerian. Phase II during the early-middle Smithian is well documented by further recovery seen among ammonoids (Brayard et al., 2009; Brühwiler et al., 2010),

conodonts (Orchard, 2007) and foraminifers (Song et al., 2011). This time interval also witnessed the local development of rather diverse community (Haig et al., 2015) and sponge bioconstructions (Brayard et al., 2011) and the presence of large-sized organisms (Brayard et al., 2010, 2015). It was associated with a relatively cooling interval (Sun et al., 2012; Romano et al., 2013) and well-oxygenated conditions (Galfetti et al., 2008; Grasby et al., 2013). This phase of diversification was followed by a severe extinction in the late Smithian (Orchard, 2007; Brayard et al., 2009; Stanley, 2009), seemingly related to high temperatures and anoxia (Sun et al., 2012; Song et al., 2012; Grasby et al., 2013). At that time, foraminifers only show a diversity low point, but no real extinction (Song et al., 2011). The Phase III diversification occurred rapidly after the late Smithian event and is seen among both nektonic and benthic forms (Brayard et al., 2009, 2017; Stanley, 2009; Song et al, 2011; Chen et al, 2015; Hautmann et al., 2013). It also witnessed the appearance of top-level predators in the fossil record (e.g. Scheyer et al. 2014; Motani et al., 2015). The Phase III diversification is associated with a cooling trend (Sun et al., 2012; Romano et al., 2013) and with the end of anoxic events characterized by the widespread occurrence of marine red beds (Song et al., 2017).

As a whole, regional environmental fluctuations controlled the recovery in space and time. The fitful recovery model gets more and more strong evidences than delayed claims, at the same time, the deteriorative environment conditions are clarified to be recurrent (e.g. Sun et al., 2012; Song et al., 2012; Grasby et al., 2013; Huang et al., 2017). The differences between benthic and nektonic/pelagic organisms recovery

patterns and underlying processes are still unclear, but are probably related to physiology variations (Bambach et al., 2002), intrinsic evolutionary rates (Stanley, 2009), and biological adaptation and competition rates (Hautmann et al., 2015). More exhaustive integrated works (paleontological and environmental) within a high-time resolution are necessary to decipher spatiotemporally heterogeneous recovery patterns among different lineages.

CONCLUSION

New evidence from two sections in South China has revealed relatively high diversity levels of ammonoids, bivalves, brachiopods, conodonts, foraminifers and gastropods during the late Griesbachian. These high diversity levels are associated with unusually well-oxygenated conditions for this period. The nektonic taxa show more stronger diversity rebound than benthic forms, possibly due to their ecology (tiering, stronger mobility) or evolutionary factors (ammonoids show much higher origination rates than benthic mollusks (Brayard et al., 2009)). Our results show a spatiotemporally heterogeneous recovery pattern linked to redox conditions, in both benthic and nektonic communities in the investigated sections in South China. In contrast to the notion of persistently harsh environmental conditions during the Early Triassic, our results suggest that there was a regionally variable recovery pattern after the PTME, linked to amelioration of environmental stresses, with three main high diversity phases during the late Griesbachian-early Dienerian, early-middle Smithian and Spathian.

ACKNOWLEDGMENTS

We thank Arnaud Brayard for participating in the determination of ammonoids,

and discussion of biostratigraphy and interpretations, Daoliang Chu for helpful discussions and Yunfei Huang for suggestions on the identification of bivalves. We appreciate comments from Ganqing Jiang, Guang R. Shi, and two anonymous reviewers that have greatly improved the quality of this paper. This study is supported by the National Natural Science Foundation of China (41622207, 41672016, 41530104, 41661134047) and the 111 Project (B08030). This is a contribution to the IGCP-630.

REFERENCES CITED

Algeo, T.J., Ellwood, B., Nguyen, T.K.T., Rowe, H., and Maynard, J.B., 2007, The Permian-Triassic boundary at Nhi Tao, Vietnam: Evidence for recurrent influx of sulfidic watermasses to a shallow-marine carbonate platform: Palaeogeography, Palaeoclimatology, Palaeoecology, v. 252, p. 304–327, doi:10.1016/j.palaeo.2006.11.055.

Algeo, T., Shen, Y., Zhang, T., Lyons, T., Bates, S., Rowe, H., and Nguyen, T.K.T., 2008, Association of ^{34}S - depleted pyrite layers with negative carbonate $\delta^{13}C$ excursions at the Permian - Triassic boundary: Evidence for upwelling of sulfidic deep - ocean water masses: Geochemistry, Geophysics, Geosystems, v. 9, no. 4, p. 1–10, doi:10.1029/2007GC001823.

Algeo, T.J., Chen, Z.Q., Fraiser, M.L., and Twitchett, R.J., 2011, Terrestrial-marine teleconnections in the collapse and rebuilding of Early Triassic marine ecosystems: Palaeogeography, Palaeoclimatology, Palaeoecology v. 308, p. 1–11, doi:10.1016/j.palaeo.2011.01.011.

Bagherpour, B., Bucher, H., Baud, A., Brosse, M., Vennemann, T., Martini, R., and

441 Guodun, K., 2017, Onset, development, and cessation of basal Early Triassic
442 microbialites (BETM) in the Nanpanjiang pull-apart Basin, South China
443 Block: Gondwana Research, v. 44, p. 178–204, doi:10.1016/j.gr.2016.11.013
444 (2016).
445 Bai, R., Dai, X., and Song, H., 2017, Conodont and ammonoid biostratigraphies around
446 the Permian-Triassic boundary from the Jianzishan of South China: Journal of
447 Earth Science, v. 28, no. 4, p. 595–613, doi:10.1007/s12583-017-0754-4.
448 Bambach, R.K., Knoll, A.H., and Sepkoski, J.J., 2002, Anatomical and ecological
449 constraints on Phanerozoic animal diversity in the marine realm: Proceedings of
450 the National Academy of Sciences, v. 99, no. 10, p. 6854–6859, doi:
451 10.1073/pnas.092150999.
452 Bond, D.P., and Wignall, P.B., 2010, Pyrite framboid study of marine Permian-Triassic
453 boundary sections: a complex anoxic event and its relationship to
454 contemporaneous mass extinction: Geological Society of America Bulletin, v. 122,
455 no. 7–8, p. 1265-1279, doi:10.1130/B30042.1.
456 Brayard, A., and Bucher, H., 2008, Smithian (Early Triassic) ammonoid faunas from
457 northwestern Guangxi (South China): taxonomy and biochronology: Fossils and
458 Strata, v. 55, p. 1–184.
459 Brayard, A., Escarguel, G., Bucher, H., Monnet, C., Brühwiler, T., Goudemand, N.,
460 Galfetti, T., and Guex, J., 2009, Good genes and good luck: ammonoid diversity
461 and the end-Permian mass extinction: Science, v. 325, no. 5944, p. 1118–1121,
462 doi:10.1126/science.1174638.

463 Brayard, A., Nützel, A., Stephen, D.A., Bylund, K.G., Jenks, J., and Bucher, H., 2010,
464 Gastropod evidence against the Early Triassic Lilliput effect: Geology, v. 38, no.
465 2, p. 147–150, doi:10.1130/G30553.1.
466 Brayard, A., Vennin, E., Olivier, N., Bylund, K.G., Jenks, J., Stephen, D.A., Bucher, H.,
467 Hofmann, R., Goudemand, N., and Escarguel, G., 2011, Transient metazoan reefs
468 in the aftermath of the end-Permian mass extinction: Nature Geoscience, v. 4, no.
469 10, p. 693–697, doi:10.1038/ngeo1264.
470 Brayard, A., Bylund, K.G., Jenks, J.F., Stephen, D.A., Olivier, N., Escarguel, G., Fara,
471 E., and Vennin, E., 2013, Smithian ammonoid faunas from Utah: implications for
472 Early Triassic biostratigraphy, correlation and basinal paleogeography: Swiss
473 Journal of Palaeontology, v. 132, no. 2, p. 141–219, doi: 10.1007/s13358-013-
474 0058-y.
475 Brayard, A., Meier, M., Escarguel, G., Fara, E., Nützel, A., Olivier, N., Bylund, K.G.,
476 Jenks, J. F., Stephen, D. A., Hautmann, M., Vennin, E., and Bucher, H., 2015, Early
477 Triassic Gulliver gastropods: Spatio-temporal distribution and significance for
478 biotic recovery after the end-Permian mass extinction: Earth-Science Reviews, v.
479 146, p. 31–64, doi:10.1016/j.earscirev.2015.03.005.
480 Brayard, A., Krumenacker, L.J., Botting, J.P., Jenks, J.F., Bylund, K.G., Fara, E.,
481 Vennin, E., Olivier, N., Goudemand, N., Saucede, T., Charbonnier, S., Romano,
482 C., Doguzhaeva, L., Thuy, B., Hautmann, M., Stephen, D.A., Thomazo, C., and
483 Escarguel, G., 2017, Unexpected Early Triassic marine ecosystem and the rise of
484 the Modern evolutionary fauna: Science Advances, v. 3, no. 2, p. e1602159, doi:

485 10.1126/sciadv.1602159.
486 Brönnimann, P., Zaninetti, L., and Bozorgnia, F., 1972, Triassic (Skythian) smaller
487 foraminifera from the Elika Formation of the central Alborz, northern Iran, and
488 from the Siusi Formation of the Dolomites, northern Italy: Mitteilung Gesellschaft
489 der Geologie und Bergsbaustudenten, Innsbruck, v. 21, p. 861-884.
490 Brosse, M., Bucher, H., Bagherpour, B., Baud, A., Frisk, Å. M., Guodun, K.,
491 Goudemand, N., and Hautmann, M., 2015, Conodonts from the Early Triassic
492 microbialite of Guangxi (South China): implications for the definition of the base
493 of the Triassic System: Palaeontology, v. 58, no. 3, p. 563–584, doi:
494 10.1111/pala.12162.
495 Brühwiler, T., Brayard, A., Bucher, H., and Guodun, K, 2008, Griesbachian and
496 Dienerian (Early Triassic) ammonoid faunas from northwestern Guangxi and
497 southern Guizhou (South China): Palaeontology, v. 51, no. 5, p. 1151–1180,
498 doi:10.1111/j.1475-4983.2008.00796.x.
499 Brühwiler, T., Bucher, H., Brayard, A., and Goudemand, N., 2010, High-resolution
500 biochronology and diversity dynamics of the Early Triassic ammonoid recovery:
501 The Smithian faunas of the Northern Indian Margin: Palaeogeography,
502 Palaeoclimatology, Palaeoecology, v. 297, no. 2, p. 491–501,
503 doi:10.1016/j.palaeo.2010.09.001.
504 Chen, J., Tong, J., Song, H., Luo, M., Huang, Y., and Xiang, Y., 2015, Recovery pattern
505 of brachiopods after the Permian-Triassic crisis in South China: Palaeogeography,
506 Palaeoclimatology, Palaeoecology, v. 433, p. 91–105,

507 doi:10.1016/j.palaeo.2015.05.020.
508 Chen, Z.Q., and Benton, M.J., 2012, The timing and pattern of biotic recovery
509 following the end-Permian mass extinction: Nature Geoscience, v. 5, no. 6, p. 375–
510 383, doi:10.1038/ngeo1475.
511 Chen, Z.Q., Tong, J., Kaiho, K., and Kawahata, H., 2007, Onset of biotic and
512 environmental recovery from the end-Permian mass extinction within 1–2 million
513 years: a case study of the Lower Triassic of the Meishan section, South
514 China: Palaeogeography, Palaeoclimatology, Palaeoecology, v. 252, no. 1, p. 176–
515 187, doi:10.1016/j.palaeo.2006.11.042.
516 Chen, Z. Q., Yang, H., Luo, M., Benton, M. J., Kaiho, K., Zhao, L., Huang, Y., Zhang,
517 K., Fang, Y., Jiang, H., Qiu, H., Li, Y., Tu, C., Shi, L., Zhang, L., Feng, X., and
518 Chen, L., 2015, Complete biotic and sedimentary records of the Permian–Triassic
519 transition from Meishan section, South China: ecologically assessing mass
520 extinction and its aftermath: Earth-science reviews, v. 149, p. 67-107,
521 doi:10.1016/j.earscirev.2014.10.005.
522 Cherdyntsev, W., 1914, Foraminiferal fauna of the Permian deposits of the eastern belt
523 of European Russia. Kazan: Trudy Obshchestva Estestvoispytateley pri
524 Imperatorskomy Kazanskomy Universitety v. 46, p. 3–88 (in Russian).
525 Chu, D., Tong, J., Song, H., Benton, M.J., Song, H., Yu, J., Qiu, X., Huang, Y., and Tian,
526 L., 2015, Lilliput effect in freshwater ostracods during the Permian–Triassic
527 extinction: Palaeogeography, Palaeoclimatology, Palaeoecology, v. 435, p. 38–52,
528 doi: 10.1016/j.palaeo.2015.06.003.
529 Clarkson, M. O., Wood, R. A., Poulton, S. W., Richoz, S., Newton, R. J., Kasemann, S.
530 A., Bowyer, F., and Krystyn, L., 2016, Dynamic anoxic ferruginous conditions

531 during the end-Permian mass extinction and recovery: Nature communications, v.
532 7, p. 12236, doi:10.1038/ncomms12236.
533 Efimova, N.A., 1974, Triassic foraminifers of the northwest Caucasus and Cis-
534 Caucasus: Akademiya Nauk SSSR, Voptosy Mikropaleontologii v. 17, p. 54–83
535 (in Russian, with English abstract).
536 Erwin, D.H., 2001, Lessons from the past: biotic recoveries from mass extinctions:
537 Proceedings of the National Academy of Sciences, v. 98, no. 10, p. 5399–5403,
538 doi: 10.1073/pnas.091092698.
539 Erwin, D.H., and Pan, H., 1996, Recoveries and Radiations: Gastropods After the
540 Permo-Triassic Mass Extinction: Geological Society, London, Special
541 Publications, v. 102, no. 1, p. 223–229, doi:10.1144/GSL.SP.1996.001.01.15.
542 Feng, Q., and Algeo, T.J., 2014, Evolution of oceanic redox conditions during the
543 Permo-Triassic transition: Evidence from deepwater radiolarian facies: Earth-
544 Science Reviews, v. 137, p. 34–51, doi: 10.1016/j.earscirev.2013.12.003.
545 Feng, Z., Bao, Z. and Liu, S. 1997. Lithofacies palaeogeography of Early and Middle
546 Triassic of South China. Beijing: Petroleum Industry Press.
547 Forel, M.B., Crasquin, S., Kershaw, S., and Collin, P.Y., 2013, In the aftermath of the
548 end-Permian extinction: the microbialite refuge?: Terra Nova, v. 25, no. 2, p. 137–
549 143, doi: 10.1111/ter.12017.
550 Forel, M.B., Crasquin, S., Kershaw, S., Feng, Q., and Collin, P.Y., 2009, Ostracods
551 (Crustacea) and water oxygenation in the earliest Triassic of South China:
552 implications for oceanic events at the end-Permian mass extinction: Australian
553 Journal of Earth Sciences, v. 56, no. 6, p. 815–823,

554 doi:10.1080/08120090903002631.
555 Forel, M.B., and Crasquin, S. 2015. Comment on the Chu et al., paper “Lilliput effect
556 in freshwater ostracods during the Permian-Triassic extinction”[Palaeogeography,
557 Palaeoclimatology, Palaeoecology v. 435, p. 38–52]: Palaeogeography,
558 Palaeoclimatology, Palaeoecology, v. 440, p. 860–862,
559 doi:10.1016/j.palaeo.2015.07.051.
560 Foster, W.J., Danise, S., Price, G.D., and Twitchett, R.J., 2017, Subsequent biotic crises
561 delayed marine recovery following the late Permian mass extinction event in
562 northern Italy: PLoS One, v. 12, no. 3, p. e0172321,
563 doi:10.1371/journal.pone.0172321.
564 Foster, W.J., Danise, S., and Twitchett, R.J., 2016, A silicified Early Triassic marine
565 assemblage from Svalbard: Journal of Systematic Palaeontology, v. 15, no. 10, p.
566 851–877, doi: 10.1080/14772019.2016.1245680.
567 Fraiser, M. L., and Bottjer, D. J., 2007, Elevated atmospheric CO_2 and the delayed biotic
568 recovery from the end-Permian mass extinction: Palaeogeography,
569 Palaeoclimatology, Palaeoecology, v. 252, no. 1–2, p. 164–175,
570 doi:10.1016/j.palaeo.2006.11.041.
571 Galfetti, T., Bucher, H., Martini, R., Hochuli, P.A., Weissert, H., Crasquin-Soleau, S.,
572 Brayard, A., Goudemand, N., Brühwiler, T., and Guodun, K., 2008, Evolution of
573 Early Triassic outer platform paleoenvironments in the Nanpanjiang Basin (South
574 China) and their significance for the biotic recovery: Sedimentary Geology, v. 204,
575 no. 1–2, p. 36–60, doi:10.1016/j.sedgeo.2007.12.008.
576 Godbold, A., Schoepfer, S., Shen, S., and Henderson, C.M., 2017, Precarious

577 ephemeral refugia during the earliest Triassic: Geology, p. G38793-1, doi:
578 10.1130/G38793.1.
579 Grasby, S.E., Beauchamp, B., Embry, A., and Sanei, H., 2013, Recurrent Early Triassic
580 ocean anoxia: Geology, v. 41, no. 2, p. 175–178, doi:10.1130/G33599.1.
581 Grasby, S.E., Beauchamp, B., and Knies, J., 2016, Early Triassic productivity crises
582 delayed recovery from world's worst mass extinction: Geology, v. 44, no. 9, p.
583 779–782, doi:10.1130/G38141.1.
584 Gu, Z.W., Huang, B.Y., Chen, C.Z. and others, 1976, Fossil Lamellibranchiata of China:
585 Science Press, Beijing, p. 1–512 (in Chinese).
586 Haig, D. W., Martin, S. K., Mory, A. J., McLoughlin, S., Backhouse, J., Berrell, R. W.,
587 Kear, B. P., Hall, R., Foster, C. B., Shi, G. R., and Bevan, J. C., 2015, Early Triassic
588 (early Olenekian) life in the interior of East Gondwana: mixed marine–terrestrial
589 biota from the Kockatea Shale, Western Australia: Palaeogeography,
590 palaeoclimatology, palaeoecology, v. 417, p. 511-533,
591 doi:10.1016/j.palaeo.2014.10.01.
592 Hallam, A., 1991, Why was there a delayed radiation after the end-Palaeozoic crisis?
593 Historical Biology, v. 5, no. 2–4, p. 257–262, doi:10.1080/10292389109380405.
594 Hauer, F. von, 1850, Ueber die von Herrn Bergrath W. Fuchs in den Venetianer Alpen
595 gesammelten Fossilien: Denkschriften der Akademie der Wissenschaften,
596 Mathematisch-Naturwissenschaftliche Klasse, v. 2, p. 109–126.
597 Hautmann, M., Bagherpour, B., Brosse, M., Frisk, Å., Hofmann, R., Baud, A., Nützel,
598 A., Goudemand, N., Bucher, H., and Brayard, A., 2015, Competition in slow
599 motion: the unusual case of benthic marine communities in the wake of the end-
600 Permian mass extinction: Palaeontology, v. 58, no. 5, p. 871–901,

601 doi:10.1111/pala.12186.
602 Hautmann, M., Bucher, H., Brühwiler, T., Goudemand, N., Kaim, A., and Nützel, A.,
603 2011, An unusually diverse mollusc fauna from the earliest Triassic of South China
604 and its implications for benthic recovery after the end-Permian biotic crisis:
605 Geobios, v. 44, no. 1, p. 71–85, doi:10.1016/j.geobios.2010.07.004.
606 Hautmann, M., Smith, A.B., McGowan, A.J., and Bucher, H., 2013, Bivalves from the
607 Olenekian (Early Triassic) of south-western Utah: systematics and evolutionary
608 significance: Journal of Systematic Palaeontology, v. 11, no. 3, p. 263–293.
609 He, W.H., Shi, G.R., Twitchett, R.J., Zhang, Y., Zhang, K.X., Song, H.J., Yue, M.L.,
610 Wu, S.B., Wu, H.T., Yang, T.L., and Xiao, Y.F., 2015, Late Permian marine
611 ecosystem collapse began in deeper waters: evidence from brachiopod diversity
612 and body size changes: Geobiology, v. 13, p. 123–138, doi:10.1111/gbi.12119.
613 Hermann, E., Hochuli, P. A., Méhay, S., Bucher, H., Brühwiler, T., Ware, D., Hautmann,
614 M., Roohi, G., ur-Rehman, K., and Yaseen, A., 2011, Organic matter and
615 palaeoenvironmental signals during the Early Triassic biotic recovery: The Salt
616 Range and Surghar Range records: Sedimentary Geology, v. 234, no. 1–4, p. 19–
617 41, doi:10.1016/j.sedgeo.2010.11.003.
618 Hofmann, R., Goudemand, N., Wasmer, M., Bucher, H., and Hautmann, M., 2011, New
619 trace fossil evidence for an early recovery signal in the aftermath of the end-
620 Permian mass extinction: Palaeogeography, Palaeoclimatology, Palaeoecology, v.
621 310, no. 3-4, p. 216-226, doi:10.1016/j.palaeo.2011.07.014.
622 Hofmann, R., Hautmann, M., Brayard, A., Nützel, A., Bylund, K.G., Jenks, J.F., Vennin,

623 E., Olivier, N., Bucher, H., and Sevastopulo, G., 2014, Recovery of benthic marine
624 communities from the end-Permian mass extinction at the low latitudes of eastern
625 Panthalassa: Palaeontology, v. 57, no. 3, p. 547–589, doi: 10.1111/pala.12076.
626 Hofmann, R., Hautmann, M., and Bucher, H., 2013, A new paleoecological look at the
627 Dinwoody Formation (Lower Triassic, western USA): intrinsic versus extrinsic
628 controls on ecosystem recovery after the end-Permian mass extinction: Journal of
629 Paleontology, v. 87, no. 05, p. 854–880, doi: 10.1666/12-153.
630 Hofmann, R., Hautmann, M., and Bucher, H., 2015, Recovery dynamics of benthic
631 marine communities from the Lower Triassic Werfen Formation, northern Italy:
632 Lethaia, v. 48, no. 4, p. 474–496, doi:10.1111/let.12121.
633 Huang, Y., Chen, Z.Q., Wignall, P.B., and Zhao, L., 2017, Latest Permian to Middle
634 Triassic redox condition variations in ramp settings, South China: Pyrite framboid
635 evidence: Geological Society of America Bulletin, v. 129, no. 1–2, p. 229–243,
636 doi:10.1130/B31458.1.
637 Jiang, H., Lai, X., Sun, Y., Wignall, P.B., Liu, J., and Yan, C., 2014, Permian-Triassic
638 conodonts from Dajiang (Guizhou, South China) and their implication for the age
639 of microbialite deposition in the aftermath of the End-Permian mass extinction:
640 Journal of Earth Science, v. 25, no. 3, p. 413–430, doi: 10.1007/s12583-014-0444-
641 4.
642 Kaim, A., Nützel, A., Bucher, H., Brühwiler, T., and Goudemand, N., 2010, Early
643 Triassic (Late Griesbachian) gastropods from South China (Shanggan, Guangxi):
644 Swiss Journal of Geosciences, v. 103, no. 1, p. 121–128, doi:10.1007/s00015-

010-0005-5.

Kaim, A., Nützel, A., Hautmann, M., and Bucher, H., 2013, Early Triassic gastropods from Salt Range, Pakistan: Bulletin of Geosciences, p. 505–516, doi: 10.3140/bull.geosci.1395.

Krystyn, L., Richoz, S., Baud, A., and Twitchett, R.J., 2003, A unique Permian–Triassic boundary section from the Neotethyan Hawasina Basin, Central Oman Mountains: Palaeogeography, Palaeoclimatology, Palaeoecology, v. 191, no. 3–4, p. 329–344, doi:10.1016/S0031-0182(02)00670-3.

Lau, K. V., Maher, K., Altiner, D., Kelley, B. M., Kump, L. R., Lehrmann, D. J., Silva-Tamayo, J. C., Weaver, K. L., Yu, M. Y., and Payne, J. L., 2016, Marine anoxia and delayed Earth system recovery after the end-Permian extinction: Proceedings of the National Academy of Sciences, v. 113, no. 9, p. 2360–2365. doi.10.1073/pnas.1515080113.

Lehrmann, D. J., 1999, Early Triassic calcimicrobial mounds and biostromes of the Nanpanjiang basin, south China: Geology, v. 27, no. 4, p. 359-362.

Leonardi, P., 1935, 2.Trias inferiore delle Venezie: Memoirie degli Istituti de Geologia e Mineralogia dell'Università di Padova v. 11, p. 1–136.

Li, G., Wang, Y., Shi, G. R., Liao, W., and Yu, L., 2016, Fluctuations of redox conditions across the Permian–Triassic boundary—New evidence from the GSSP section in Meishan of South China: Palaeogeography, Palaeoclimatology, Palaeoecology, v. 448, p. 48-58, doi:10.1016/j.palaeo.2015.09.050.

Liao, W., Bond, D. P., Wang, Y., He, L., Yang, H., Weng, Z., and Li, G., 2017, An extensive anoxic event in the Triassic of the South China Block: A pyrite framboid study from Dajiang and its implications for the cause (s) of oxygen depletion: Palaeogeography, Palaeoclimatology, Palaeoecology, v. 486, p. 86-95, doi:10.1016/j.palaeo.2016.11.012.

671 Liu, L., 1964, Early Triassic bivalves from eastern Qinling, Shaanxi province: Acta
672 Palaeontologica Sinica, v. 12, no. 2, p. 312–322 (in Chinese).
673 Liu, L., Wu, Y.S., Li, Y., Liu, Q.S., Jiang, H.X., and Liu, H., 2017, Microfacies of a
674 Permian calcisponge reef in Lichuan, western Hubei, South China: Palaeoworld,
675 doi: 10.1016/j.palwor.2017.05.006.
676 Meyer, K. M., Yu, M., Jost, A. B., Kelley, B. M., and Payne, J. L., 2011, $\delta^{13}C$ evidence
677 that high primary productivity delayed recovery from end-Permian mass
678 extinction: Earth and Planetary Science Letters, v. 302, no. 3–4, p. 378–384, doi:
679 10.1016/j.epsl.2010.12.033.
680 Miklukho-Maklay, K.V., 1954, Foraminifers of the Upper Permian Deposits of the
681 Northern Caucasus: Trudy Vsesoyuznogo NauchnoIssledovatel'skogo
682 Geologicheskogo Instituta (VSEGEI). Ministerstva Geologii i Okhrani Nedr, p. 1-
683 163.
684 Motani, R., Jiang, D. Y., Chen, G. B., Tintori, A., Rieppel, O., Ji, C., and Huang, J. D.,
685 2015, A basal ichthyosauriform with a short snout from the Lower Triassic of
686 China: Nature, v. 517, no. 7535, p. 485–488, doi:10.1038/nature13866.
687 Mu, L., Zakharov, Y., Li, W. and Shen, S., 2007, Early Induan (Early Triassic)
688 cephalopods from the Daye Formation at Guiding, Guizhou Province, South
689 China: Journal of Paleontology, v. 81, no. 5, p. 858–872, doi: 0022-
690 3360/07/0081-858$03.00.
691 Nützel, A., 2005, Recovery of gastropods in the Early Triassic: Comptes Rendus
692 Palevol, v. 4, no. 6–7, p. 501–515, doi:10.1016/j.crpv.2005.02.007.
693 Orchard, M.J., 2007, Conodont diversity and evolution through the latest Permian and

694 Early Triassic upheavals: Palaeogeography, Palaeoclimatology, Palaeoecology, v.
695 252, no. 1–2, p. 93–117, doi:10.1016/j.palaeo.2006.11.037.
696 Patte, E., 1935, Fossils paleozoiques et mesodu Sud-Ouest de la Chine: Palaeontologia
697 Sinica Series B, v. 15, p. 1–50.
698 Payne, J.L., 2005, Evolutionary dynamics of gastropod size across the end-Permian
699 extinction and through the Triassic recovery interval, Paleobiology, Volume 31, p.
700 269–290.
701 Payne, J.L., Lehrmann, D.J., Wei, J., and Knoll, A.H., 2006, The Pattern and Timing of
702 Biotic Recovery from the End-Permian Extinction on the Great Bank of Guizhou,
703 Guizhou Province, China: Palaios, v. 21, no. 1, p. 63–85,
704 doi:10.2110/palo.2005.p05-12p.
705 Payne, J.L., Summers, M., Rego, B.L., Altiner, D., Wei, J., Yu, M., and Lehrmann, D.
706 J., 2011, Early and Middle Triassic trends in diversity, evenness, and size of
707 foraminifers on a carbonate platform in south China: implications for tempo and
708 mode of biotic recovery from the end-Permian mass extinction: Paleobiology, v.
709 37, no. 3, p. 409–425, doi: 10.1666/08082.1.
710 Payne, J.L., Turchyn, A.V., Paytan, A., DePaolo, D.J., Lehrmann, D.J., Yu, M., and Wei,
711 J., 2010, Calcium isotope constraints on the end-Permian mass extinction:
712 Proceedings of the National Academy of Sciences, v. 107, no. 19, p. 8543–8548,
713 doi: 10.1073/pnas.0914065107.
714 Pietsch, C., and Bottjer, D.J., 2014, The importance of oxygen for the disparate
715 recovery patterns of the benthic macrofauna in the Early Triassic: Earth-Science

716 Reviews, v. 137, p. 65–84, doi:10.1016/j.earscirev.2013.12.002.
717 Raup, D.M., 1979, Size of the Permo-Triassic bottleneck and its evolutionary
718 implications: Science, v. 206, p. 217–218.
719 Romano, C., Goudemand, N., Vennemann, T.W., Ware, D., Schneebeli-Hermann, E.,
720 Hochuli, P.A., Brühwiler, T., Brinkmann, W., and Bucher, H., 2013, Climatic and
721 biotic upheavals following the end-Permian mass extinction: Nature Geoscience,
722 v. 6, no. 1, p. 57–60, doi:10.1038/ngeo1667.
723 Sepkoski Jr, J.J., 1981, A factor analytic description of the Phanerozoic marine fossil
724 record: Paleobiology, v. 7, no. 1, p. 36–53, doi:10.1017/S0094837300003778.
725 Shigeta, Y., Zakharov, Y.D., Maeda, H., and Popov, A.M., 2009, The Lower Triassic
726 System in the Abrek Bay Area, South Primorye, Russia: Tokyo: National Museum
727 of Nature and Science, p. 1–218.
728 Scheyer, T.M., Romano, C., Jenks, J., and Bucher, H., 2014, Early Triassic marine biotic
729 recovery: the predators' perspective. Plos One, v. 9, no. 3, p. e88987,
730 doi:10.1371/journal.pone.0088987.
731 Scotese, C.R. 2001. Atlas of earth history. University of Texas at Arlington.
732 Department of Geology. PALEOMAP Project.
733 Song, H., Jiang, G., Poulton, S. W., Wignall, P. B., Tong, J., Song, H., An, Z., Chu, D.,
734 Tian, L., She, Z., and Wang, C., 2017, The onset of widespread marine red beds
735 and the evolution of ferruginous oceans: Nature Communications, v. 8, no. 1, p.
736 399, doi:10.1038/s41467-017-00502-x.
737 Song, H., Tong, J., and Chen, Z.Q., 2011, Evolutionary dynamics of the Permian–

738 Triassic foraminifer size: evidence for Lilliput effect in the end-Permian mass
739 extinction and its aftermath: Palaeogeography, Palaeoclimatology,
740 Palaeoecology, v. 308, no. 1, p. 98–110, doi:10.1016/j.palaeo.2010.10.036.
741 Song, H., Wignall, P.B., Chen, Z.Q., Tong, J., Bond, D.P.G., Lai, X., Zhao, X., Jiang,
742 H., Yan, C., Niu, Z., Chen, J., Yang, H., and Wang, Y., 2011, Recovery tempo and
743 pattern of marine ecosystems after the end-Permian mass extinction: Geology, v.
744 39, no. 8, p. 739–742, doi:10.1130/G32191.1.
745 Song, H., Wignall, P.B., Chu, D., Tong, J., Sun, Y., Song, H., He, W., and Tian, L.,
746 2014, Anoxia/high temperature double whammy during the Permian-Triassic
747 marine crisis and its aftermath: Scientific Reports, v. 4, p. 1–7,
748 doi:10.1038/srep04132.
749 Song, H., Wignall, P.B., Tong, J., Bond, D.P., Song, H., Lai, X., Zhang, K., Wang, H.
750 and Chen, Y. 2012. Geochemical evidence from bio-apatite for multiple oceanic
751 anoxic events during Permian-Triassic transition and the link with end-Permian
752 extinction and recovery: Earth and Planetary Science Letters, v. 353, no. 2012, p.
753 12–21, doi.org/10.1016/j.epsl.2012.07.005.
754 Song, H., Wignall, P.B., Tong, J., and Yin, H. 2013. Two pulses of extinction during
755 the Permian-Triassic crisis: Nature Geoscience, v. 6, no. 1, p. 52–56,
756 doi:10.1038/NGEO1649.
757 Stanley, S.M., 2009, Evidence from ammonoids and conodonts for multiple Early
758 Triassic mass extinctions: Proceedings of the National Academy of Sciences, v.
759 106, no. 36, p. 15264–15267, doi:10.1073/pnas.0907992106.

760 Stanley, S.M. 2016, Estimates of the magnitudes of major marine mass extinctions in
761 earth history: Proceedings of the National Academy of Sciences, v. 113, no. 42, p.
762 E6325–E6334, doi:10.1073/pnas.1613094113.
763 Sun, Y., Joachimski, M.M., Wignall, P.B., Yan, C., Chen, Y., Jiang, H., Wang, L., and
764 Lai, X., 2012, Lethally Hot Temperatures During the Early Triassic Greenhouse:
765 Science, v. 338, no. 6105, p. 366–370, doi:10.1126/science.1224126.
766 Tian, L., Tong, J., Algeo, T.J., Song, H., Song, H., Chu, D., Shi, L., and Bottjer, D.J.
767 2014. Reconstruction of Early Triassic ocean redox conditions based on
768 framboidal pyrite from the Nanpanjiang Basin, South China: Palaeogeography,
769 Palaeoclimatology, Palaeoecology, v. 412, p. 68–79,
770 doi.org/10.1016/j.palaeo.2014.07.018.
771 Tong, J., Zuo, J., and Chen, Z.Q., 2007, Early Triassic carbon isotope excursions from
772 South China: Proxies for devastation and restoration of marine ecosystems
773 following the end-Permian mass extinction: Geological Journal, v. 42, p. 371–389,
774 doi:10.1002/gj.1084.
775 Twitchett, R.J., 2007, The Lilliput effect in the aftermath of the end-Permian extinction
776 event: Palaeogeography, Palaeoclimatology, Palaeoecology, v. 252, p. 132–144,
777 doi:10.1016/j.palaeo.2006.11.038.
778 Twitchett, R.J., Krystyn, L., Baud, A., Wheeley, J.R., and Richoz, S., 2004, Rapid
779 marine recovery after the end-Permian mass-extinction event in the absence of
780 marine anoxia: Geology, v. 32, no. 9, p. 805–808, doi:10.1130/G20585.1.
781 Wang, F., Chen, J., Dai, X., and Song, H., 2017, A new Dienerian (Early Triassic)

782 brachiopod fauna from South China and implications for biotic recovery after the
783 Permian-Triassic extinction: Papers in Palaeontology, v. 3, no. 3, p. 425–439, doi:
784 10.1002/spp2.1083.
785 Ware, D., Bucher, H., Brayard, A., Schneebeli-Hermann, E., and Brühwiler, T., 2015,
786 High-resolution biochronology and diversity dynamics of the Early Triassic
787 ammonoid recovery: The Dienerian faunas of the Northern Indian Margin:
788 Palaeogeography, Palaeoclimatology, Palaeoecology, v. 440, p. 363–373,
789 doi:10.1016/j.palaeo.2015.09.013.
790 Wasmer, M., Hautmann, M., Hermann, E., Ware, D., Roohi, G., Ur-Rehman, K., Yaseen,
791 A., and Bucher, H., 2012, Olenekian (Early Triassic) bivalves from the Salt Range
792 and Surghar Range, Pakistan: Palaeontology, v. 55, no. 5, p. 1043–1073,
793 doi:10.1111/j.1475-4983.2012.01176.x.
794 Wignall, P.B., Bond, D.P.G., Sun, Y.D., Grasby, S.E., Beauchamp, B., Joachimski,
795 M.M., and Blomeier, D.P.G., 2016, Ultra-shallow marine anoxia in an Early
796 Triassic shallow-marine clastic ramp (Spitsbergen) and the suppression of benthic
797 radiation: Geological Magazine, v. 153, p. 316–331,
798 doi:10.1017/S0016756815000588.
799 Wignall, P. B., and Twitchett, R. J., 1996, Oceanic anoxia and the end-Permian mass
800 extinction: Science, v. 272, no. 5265, p. 1155–1158.
801 Xiao, Y., Suzuki, N., and He, W., 2017, Water depths of the latest Permian
802 (Changhsingian) radiolarians estimated from correspondence analysis: Earth-
803 Science Reviews, v. 173, p. 141–158, doi:10.1016/j.earscirev.2017.08.012.
804 Xu, G., 1988, Early Triassic cephalopods from Lichuan, Western Hubei: Acta

805 Palaeontologica Sinica, v. 27, no. 4, p. 437–456, (in Chinese, with English
806 summary).
807 Yang, H., Chen, Z.Q., Wang, Y., Tong, J., Song, H., and Chen, J., 2011, Composition
808 and structure of microbialite ecosystems following the end-Permian mass
809 extinction in South China: Palaeogeography, Palaeoclimatology, Palaeoecology, v.
810 308, no. 1–2, p. 111–128, doi:10.1016/j.palaeo.2010.05.029.
811 Yin, H., Jiang, H., Xia, W., Feng, Q., Zhang, N., and Shen, J., 2014, The end-Permian
812 regression in South China and its implication on mass extinction: Earth-Science
813 Reviews, v. 137, p. 19–33, doi: 10.1016/j.earscirev.2013.06.003.
814 Zhang, K., Tong, J., Shi, G. R., Lai, X., Yu, J., He, W., Peng, Y., and Jin, Y., 2007, Early
815 Triassic conodont–palynological biostratigraphy of the Meishan D Section in
816 Changxing, Zhejiang Province, South China: Palaeogeography,
817 Palaeoclimatology, Palaeoecology, v. 252, no. 1–2, p. 4–23,
818 doi:10.1016/j.palaeo.2006.11.031.
819 Zheng, Z., 1981, Uppermost Permian (Changhsingian) ammonoids from Western
820 Guizhou: Acta Palaeontologica Sinica, v. 20, no. 2, p. 107–114, (in Chinese, with
821 English abstract).
822
823 **FIGURE CAPTIONS**

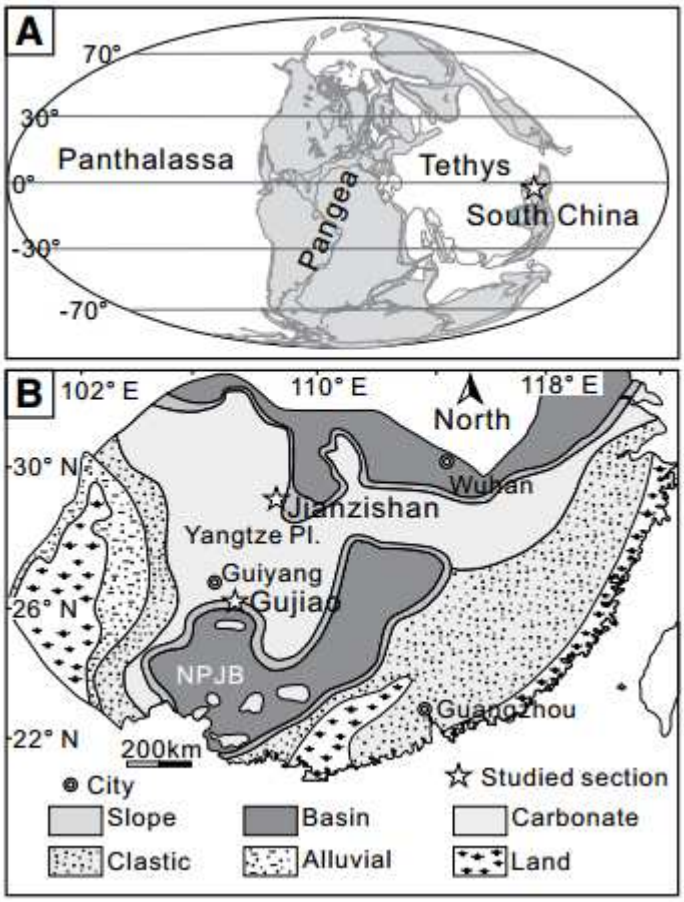

824

825 Figure 1. A. Early Triassic paleogeography, modified from Scotese (2001). B. Early

826 Triassic paleogeographic map of South China, modified from Feng et al. (1997). PL.

827 platform; NPJB. Nanpanjiang Basin.

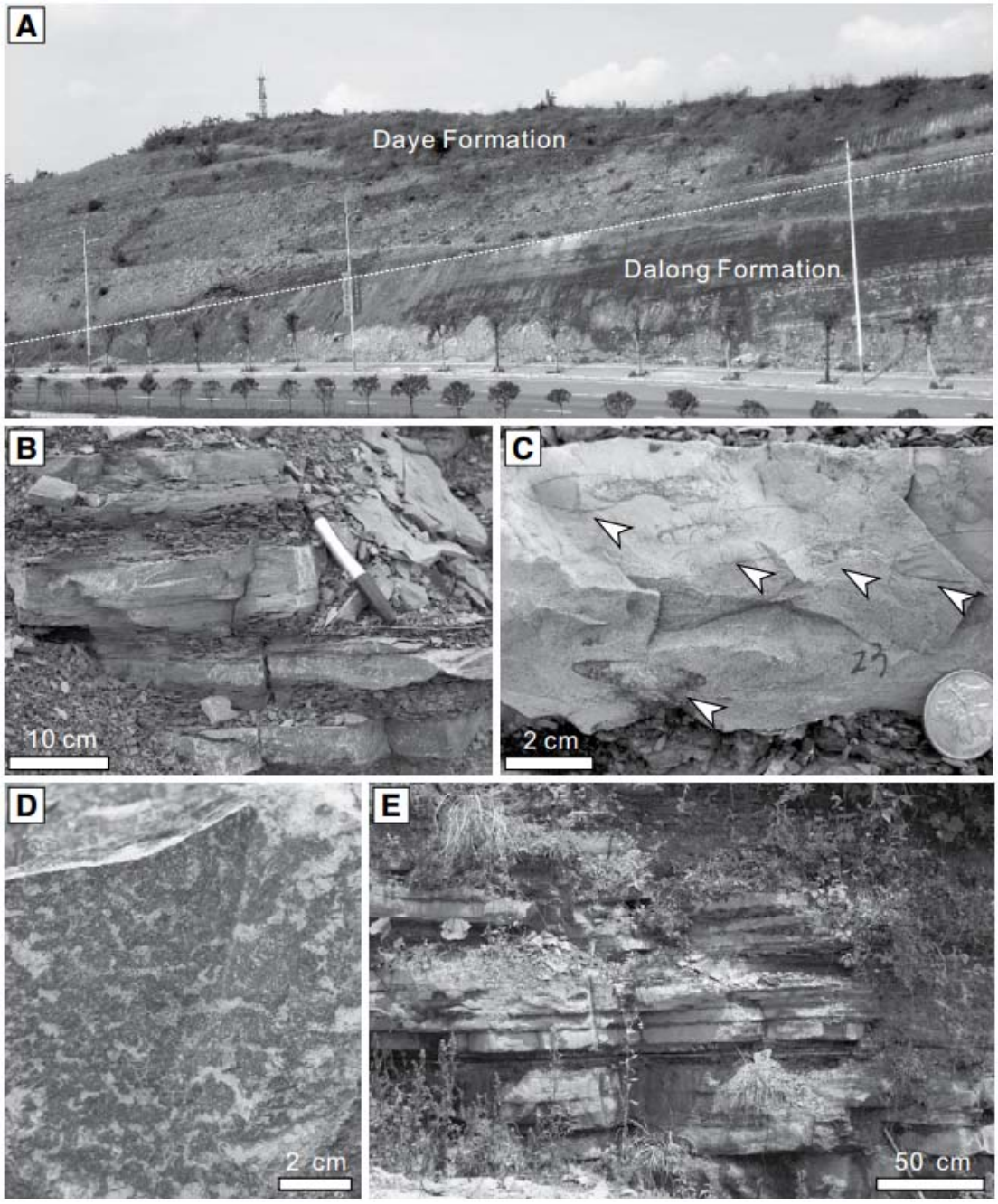

828

829 Figure 2. A. Landscape view of the Gujiao section. B. Laminated marlstones alternated
830 with black shales of the Daye Formation at Gujiao. C. Light gray marlstones with
831 abundant ammonoids (indicated by white arrows). D. Microbialites from the lower
832 most of the Daye Formation at Jianzishan. E. Mudstones alternating with shales
833 overlying the microbialites at Jianzishan.

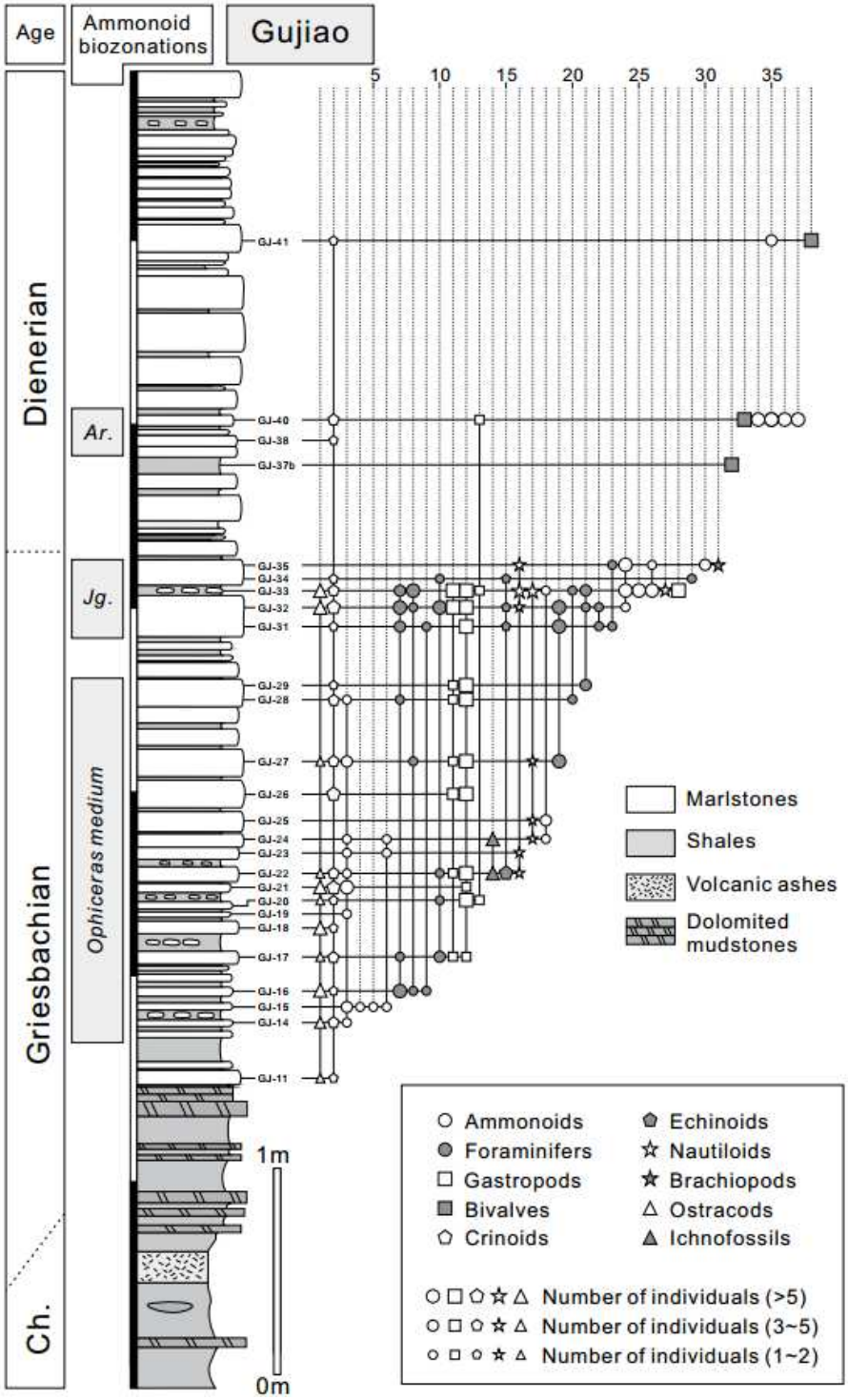

834

835 Figure 3. Fossil occurrences in the Gujiao section. See Table 1 for fossil list. Ch.

836 Changhsingian; *Ar*. *Ambites radiatus* bed; *Jg*. *Jieshaniceras guizhouense* beds.

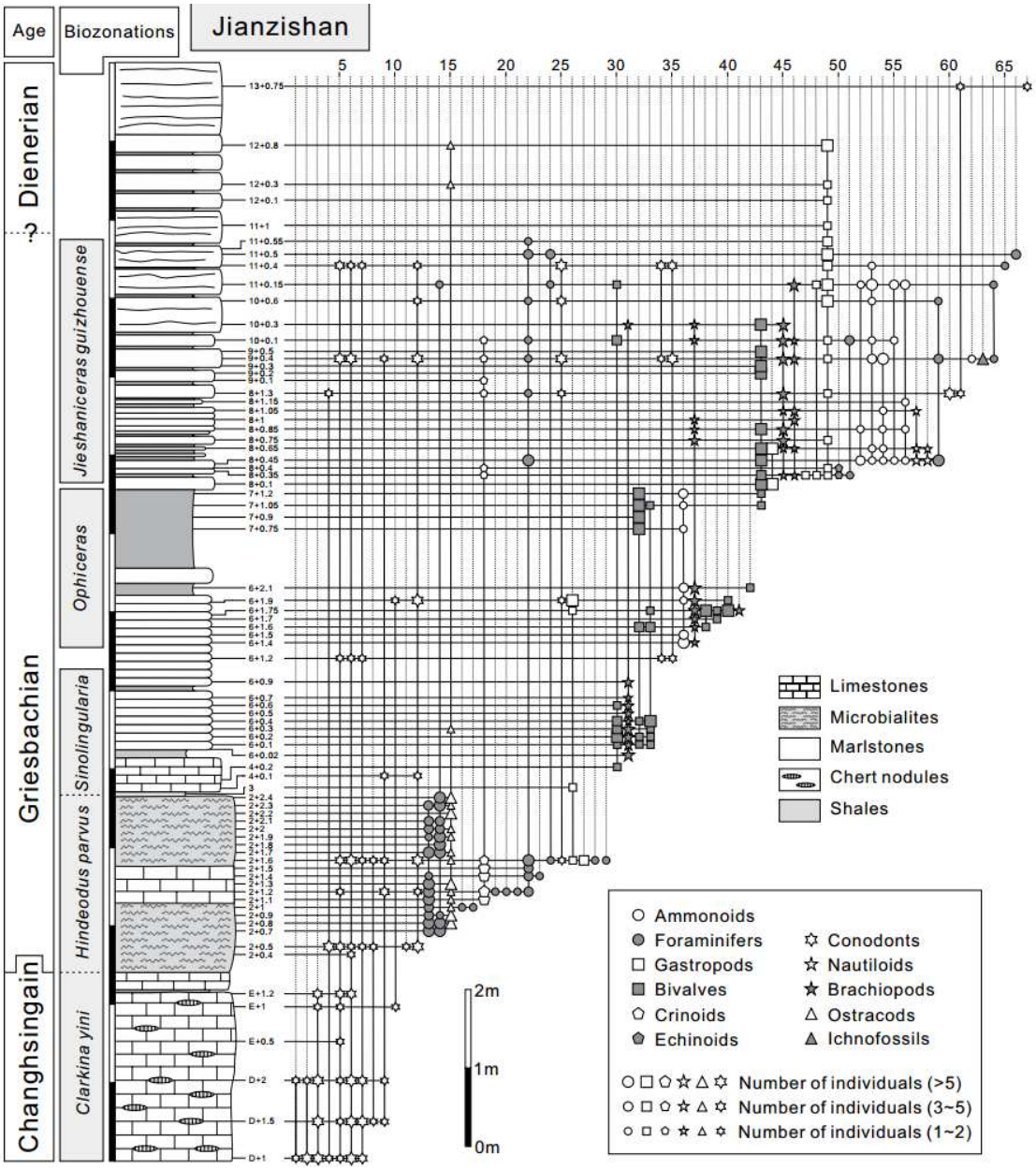

837

838 Figure 4. Fossil occurrences in the Jianzishan section. Conodont data and part of

839 ammonoid data are from Bai et al. (2017). Brachiopod data are from Wang et al. (2017).

840 See Table 2 for fossil list.

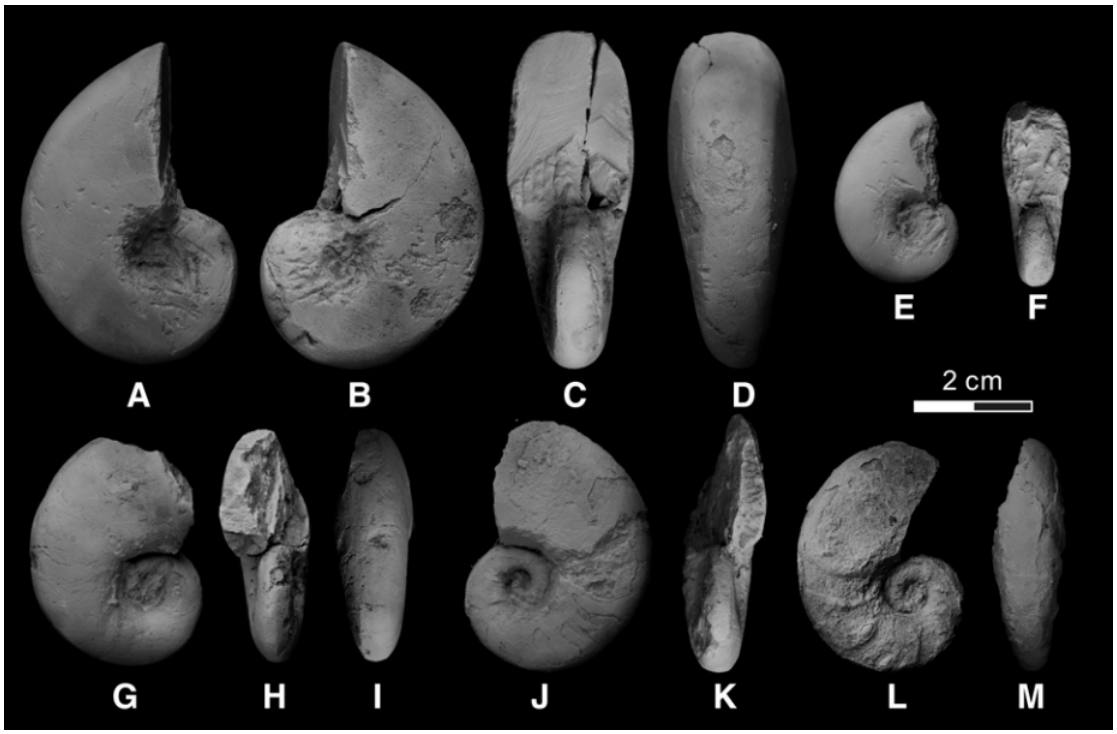

841

842 Figure 5. Nautiloids from bed GJ-33, Gujiao section. A-D. *Xiaohenautilus sinensis* Xu,

843 1988; E-F. *Xiaohenautilus sinensis* Xu, 1988; G-I. *Xiaohenautilus huananensis* Xu,

844 1988; J-K. *Xiaohenautilus huananensis* Xu, 1988; L M. undetermined nautiloid.

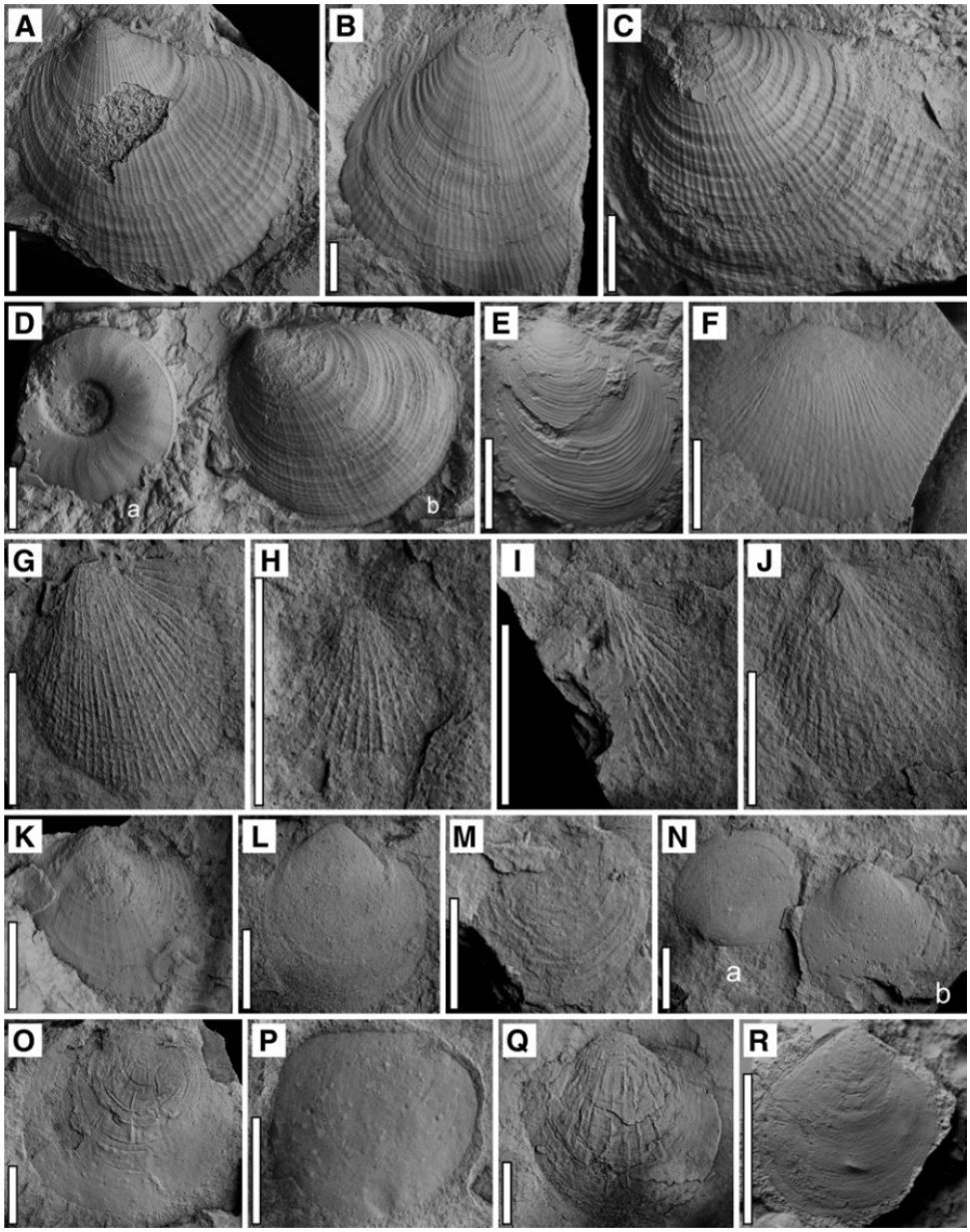

Figure 6. Mollusks from the Gujiao and Jianzishan sections. Scale bar is 1 cm. A-C. *Claraia radialis* (Leonardi, 1935), A, left valve, from GJ-40, B, right valve, from GJ-40, C, left valve, from GJ-40; D. a. *Ambites radiatus* (Brühwiler, Brayard, Bucher and Kuang, 2008), b. *Claraia radialis* (Leonardi, 1935), left valve, from GJ-40; E. *Claraia aurita* (von Hauer, 1850), left valve, from GJ-41; F. *Claraia stachei* (Patte, 1935), left valve, from GJ-37b; G-J. *Eumorphotis venetiana* (von Hauer, 1850), G, left valve, from JZS-6+0.3, H, left valve, from JZS-6+0.35, I, left valve, from JZS-6+0.3, J, left valve,

from JZS-6+0.3; K-N. *Claraia wangi* (Patte, 1935), K, left valve, from JZS-6+0.45, L, left valve, from JZS- 7+0.75, M, left valve, from JZS-7+1.05, N, a. left valve, b. right value, from JZS-7+1.2; O-Q. *Claraia zhenanica* Chen and Liu in Liu, 1964, O, right valve, from JZS-8+0.65, P, right valve, from JZS-8+0.65, Q, left valve, from JZS-9+0.2; R. *Scythentolium scutigerulus* Hautmann et al., 2011, left valve, From JZS-6+1.9.

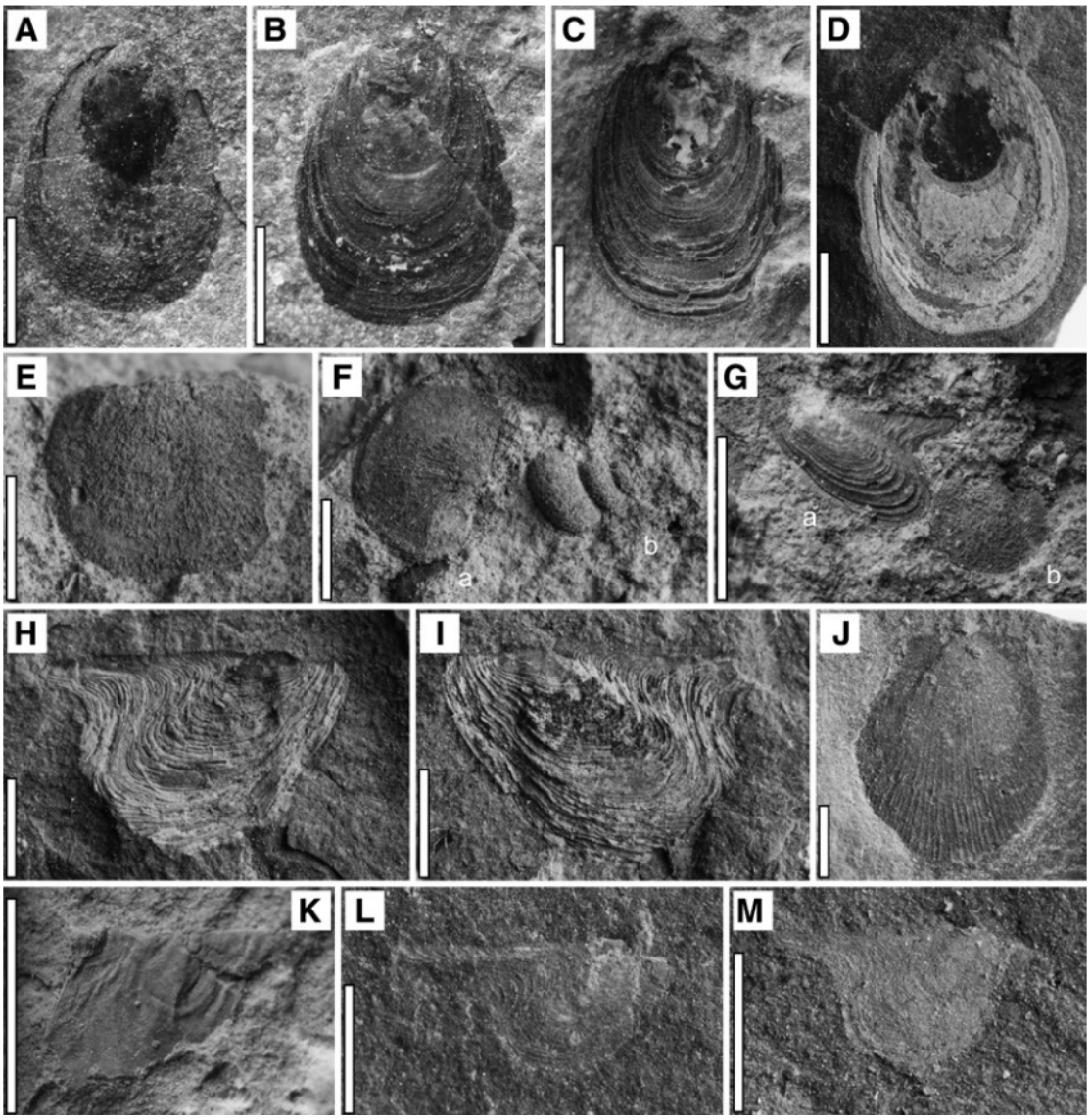

Figure 7. Brachiopods, bivalves and gastropods from the Jianzishan section. The scale bar is 2 mm. A-D. *Sinolingularia* sp. indet.; A, from JZS-6+0.02; B, from JZS-6+0.3; C, from JZS- 6+0.9; D, from JZS-10+0.3; E. *Crurithyris* sp. indet., from JZS-6+1.9; F.

a. *Crurithyris* sp. indet., b. ?*Pseudomurchisonia* sp. indet., from JZS-6+1.9; G. a. *Pteria ussurica variabilis* Chen and Lan in Gu et al, 1976, left valve; b. *Crurithyris* sp. indet., from JZS-6+1.75; H. *Pteria ussurica variabilis* Chen and Lan in Gu et al, 1976, left valve, external mold, from JZS-6+1.75; I. *Pteria ussurica variabilis* Chen and Lan in Gu et al, 1976, left valve, from JZS-6+1.75; J. *Eumorphotis* sp. indet., left valve, from JZS-6+1.75; K. *Eumorphotis* sp. indet., right valve, from JZS-6+1.7; L. *Pteria ussurica variabilis* Chen and Lan in Gu et al, 1976, right valve, from JZS-6+1.75; M. *Pteria ussurica variabilis* Chen and Lan in Gu et al, 1976, right valve, from JZS-6+1.75.

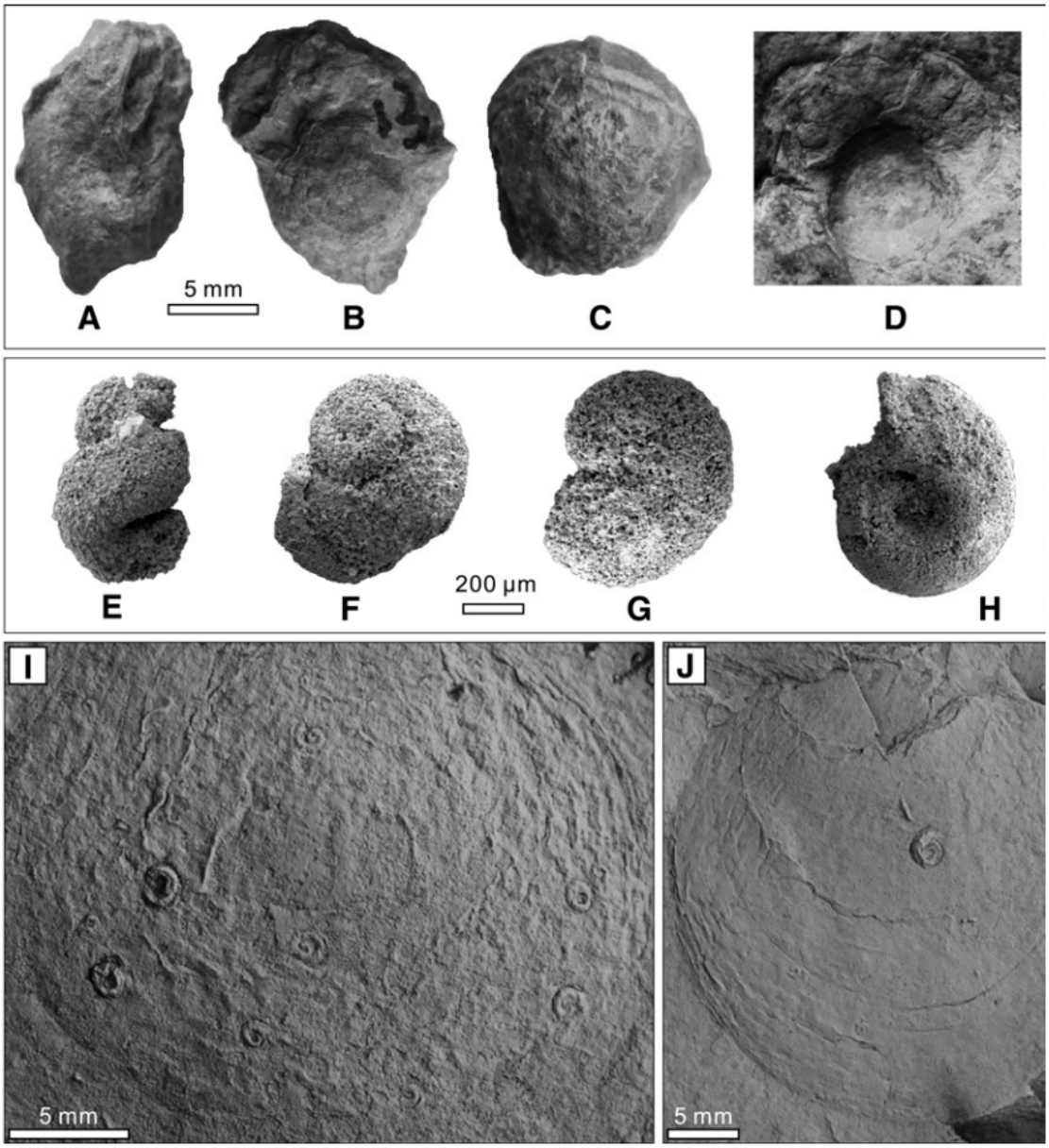

Figure 8. Gastropods and microconchids from the Gujiao and Jianzishan sections. A-D. Bellerophontidae gen. indet., from bed GJ-33; E. undetermined Gastropod A., from bed JZS-6+1.9; F-G. ?*Naticopsis* sp. indet., from bed JZS-6+1.9; H. Bellerophontidae gen. indet., from bed JZS-6+1.9. I-J, epizoan microconchids on *Claraia* shells, from bed JZS-8+0.65.

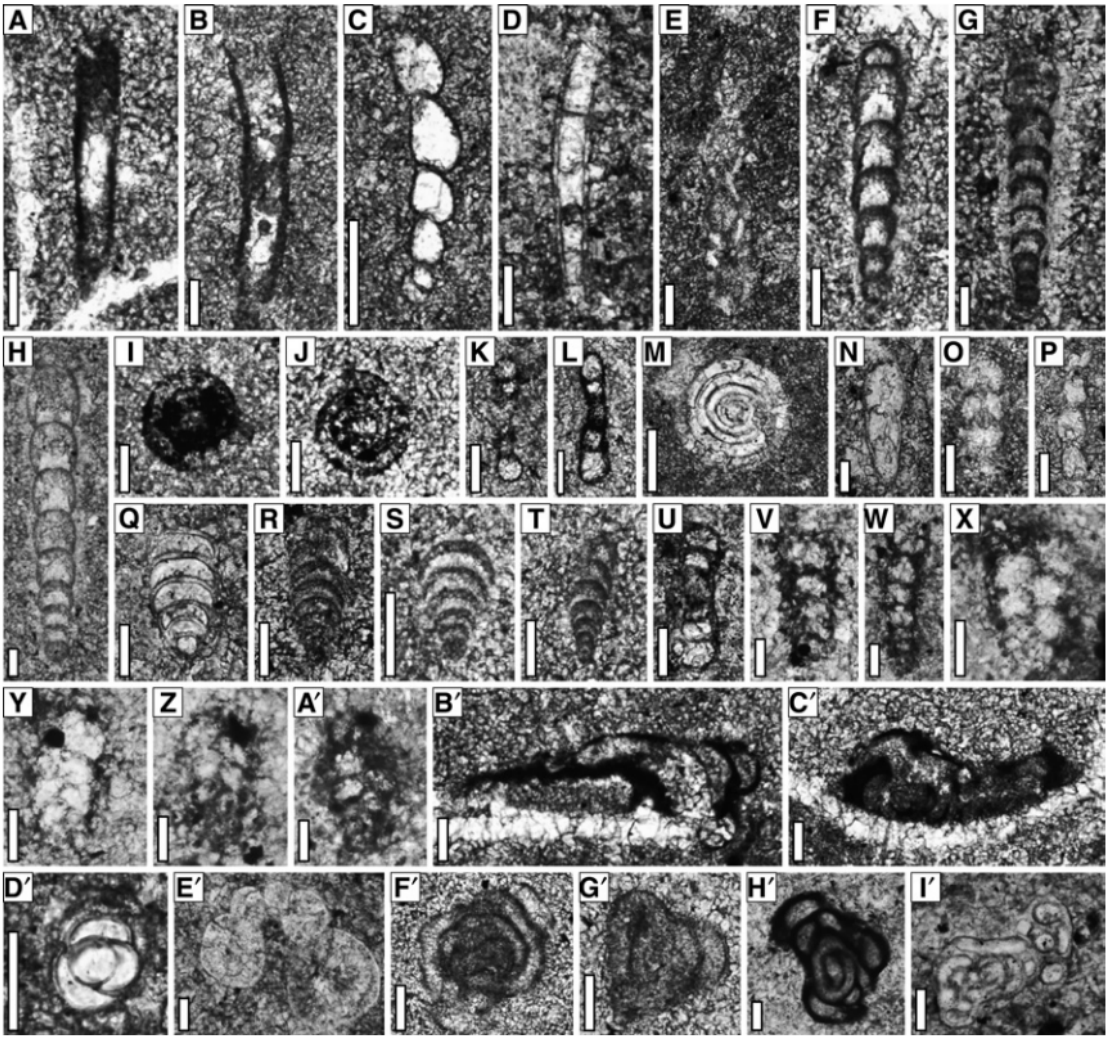

Figure 9. Foraminifers from the Gujiao and Jianzishan sections. The scale bar is 50 μm. A-B. *Earlandia* sp. indet., from JZS-2+0.7; C. *Dentalina* sp. indet., from JZS-2+1; D. *Tezaquina* sp. indet., from JZS-2+1.2; E. *Vervilleina* sp., indet., from JZS-11+0.4; F-H. *Nodosinelloides sagitta* (Miklukho-Maklay, 1954), F-G, from JZS-11+0.5, H, from GJ-28; I-L, *Postcladella kalhori* (Brönnimann, Zaninetti and Bozorgnia, 1972), I-J, from JZS-2+0.7, K-L from JZS-2+2.3; M. *Ammodiscus* sp. indet., from JZS-2+1; N. "*Nodosaria*" sp. indet., from JZS-2+1.2; O. "*Nodosaria*" *elabugae* Cherdyntsev, 1914, from JZS-2+1.6; P. "*Nodosaria*" *skyphica* Efimova, 1974, from JZS-2+1.6; Q-S. *Geinitzina* sp. indet., Q, from JZS-2+1.6, R-S, from JZS-11+0.4; T. *Frondina* sp. indet.,

from JZS-9+0.4; U. *Hemigordius* sp. indet., from JZS-2+1.2; V-W. ?*Dagmarita* sp. indet., V, from GJ-29, W, from GJ-33; X-A'. *Gaudryina* sp. indet., X-Z, from GJ-32, A', from GJ-33; B'-C'. *Tolypammina* sp. indet., from JZS-9+0.4; D'. ?*Duotaxis* sp. indet., from JZS-2+1.4; E'. *Duotaxis* sp. indet., from GJ-28; F'-I'. *Glomospira* sp. indet., F'-G', from JZS-10+0.1, H' from JZS-8+0.35, I' from GJ-31.

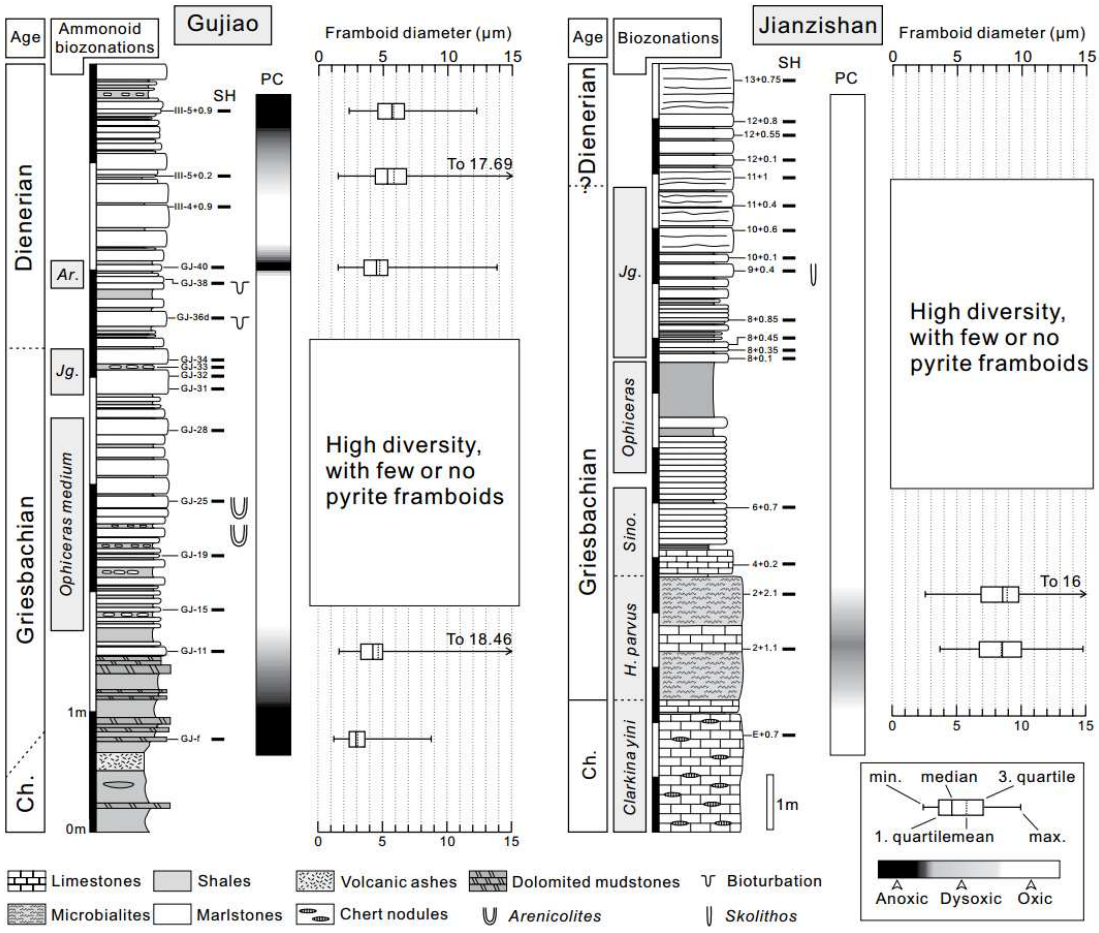

Figure 10. Griesbachian-Dienerian paleoredox conditions of the Gujiao and Jianzishan sections. Only five samples yield pyrite framboids at Gujiao, and two at Jianzishan. SH: pyrite sample horizon. PC: Paleoredox conditions. Biozonations abbreviation. *Jg*. *Jieshaniceras guizhouense* beds; *Ar*. *Ambites radiatus* bed; *H*. *Hindeodus*; *Sino*. *Sinolingularia* beds.

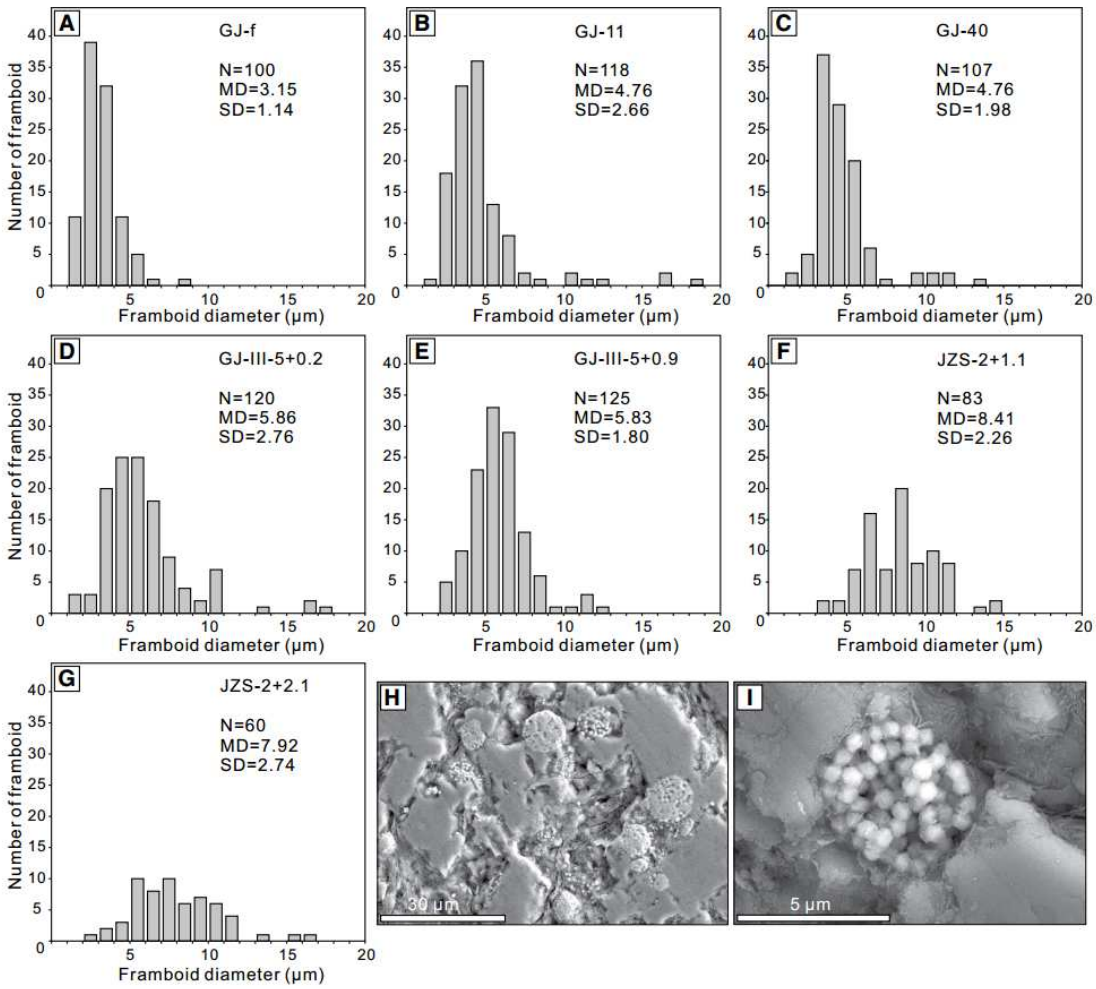

Figure 11. A-G. Size distributions of pyrite framboids. H-I. SEM photos of typical pyrite framboids, from sample GJ-III- 5+0.9.

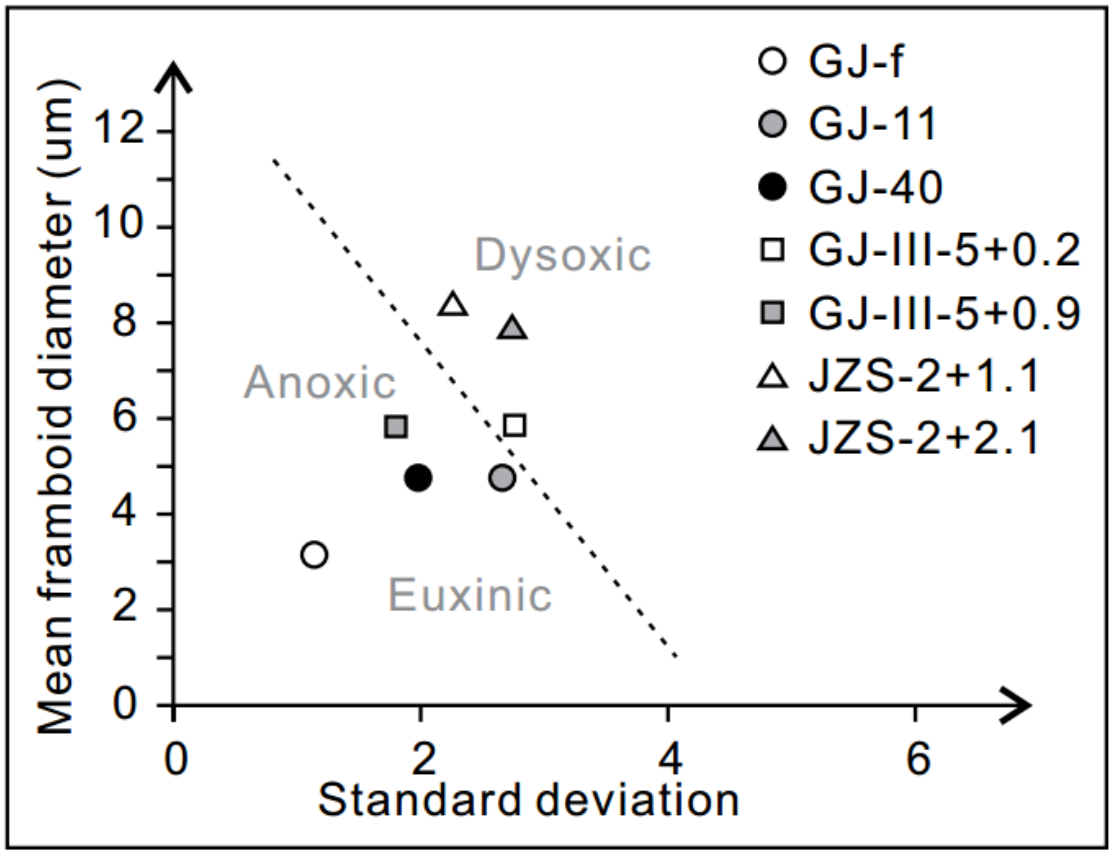

Figure 12. Mean diameter versus standard deviation of pyrite framboids. The dotted line separating euxinic/anoxic from dysoxic facies is from Bond and Wignall (2010) and Tian et al., (2014) and is derived from measurements in modern environments.

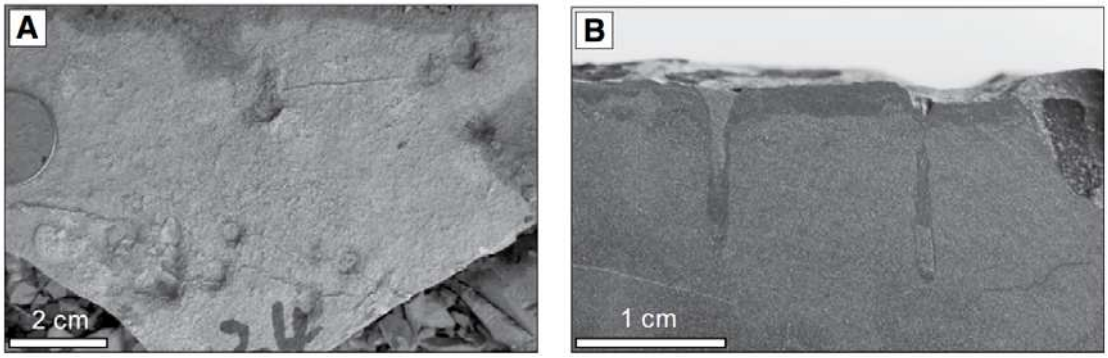

Figure 13. Ichnofossils from the Gujiao and Jianzishan sections. A, *Arenicolites* isp., from bed GJ-24. B, *Skolithos* isp., from bed JZS-9+0.4.

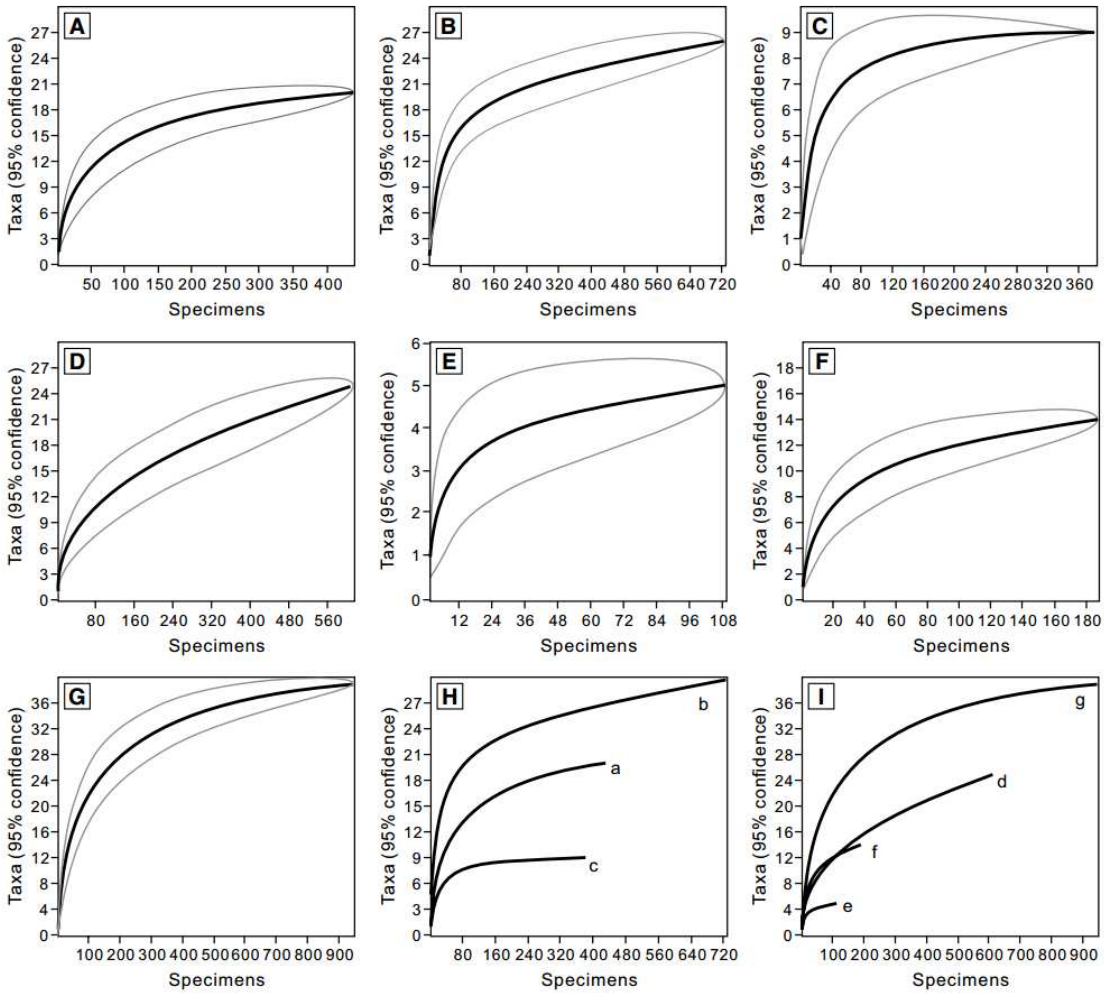

Figure 14. Rarefaction analyses for each analyzed zone or beds. The grey lines indicate 95% confidence intervals. The *Jieshaniceras guizhouense* beds in both sections contain the highest taxonomic richness. A, *Ophiceras medium* beds, Gujiao section. B, *Jieshaniceras guizhouense* beds, Gujiao section. C, *Ambites radiatus* bed, Gujiao section. D, *Hindeodus parvus* Zone, Jianzishan section. E, *Sinolingularia* beds, Jianzishan section. F, *Ophiceras medium* beds, Jianzishan section. G, *Jieshaniceras guizhouense* beds, Jianzishan section. H, rarefaction for each bed at Gujiao, a, *Ophiceras medium* beds; b, *Jieshaniceras guizhouense* beds; c, *Ambites radiatus* bed. I, rarefaction for each biozone/assemblage at Jianzishan, d, *Hindeodus parvus* Zone, e, *Sinolingularia* beds, f, *Ophiceras medium* beds, g, *Jieshaniceras guizhouense* beds.

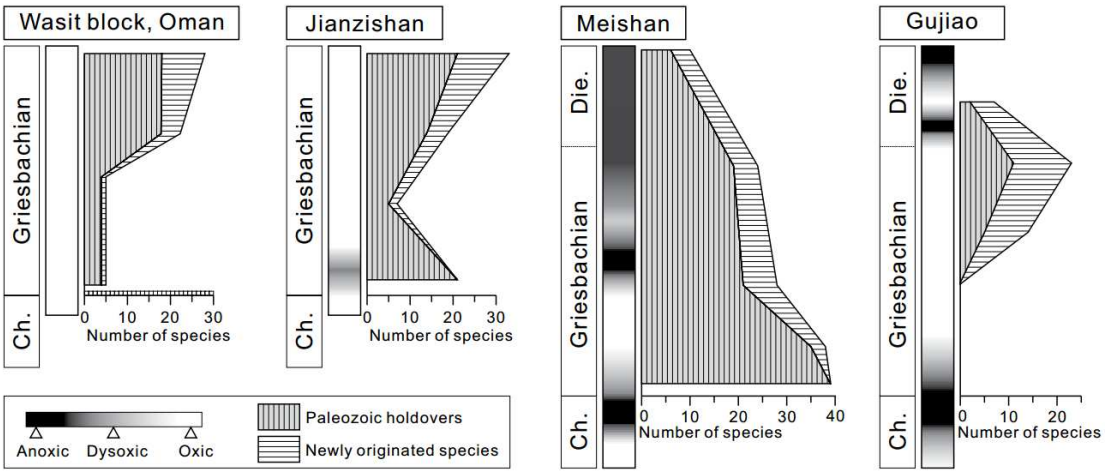

Figure 15. Correlation of paleoredox conditions and taxonomic richness of Paleozoic holdovers and new originated species. The redox conditions of Wasit block, Oman is from Clarkson et al. (2016) and the paleontological data are from Twitchett et al. (2004). The redox conditions of Meishan is from Chen et al. (2014) and Li et al. (2016) and the paleontological data is from Chen et al. (2007) and Song et al. (2013). Ch. Changhsingian; Die. Dienerian.